Bioorganic Chemistry 168 (2026) 109364

Contents lists available at ScienceDirect

Bioorganic Chemistry

journal homepage: www.elsevier.com/locate/bioorg

A series of 4-thiomorpholinophenyl-thiosemicarbazones as cholinesterase inhibitors with anti-neuroblastoma effects

Hina Aftab [a], Furkan Çakır [b], Gurbet Çelik Turgut [c], Nastaran Sadeghian [d], Rima D. Alharthy [e], Parham Taslimi [d], Alaattin Şen [f], Magdi E.A. Zaki [g], Sobhi M. Gomha [h,*], Javid Hussain [i], Zahid Shafiq [a], Halil Şenol [b,*]

[a] Institute of Chemical Sciences, Bahauddin Zakariya University, 60800 Multan, Pakistan
[b] Department of Pharmaceutical Chemistry, Faculty of Pharmacy, Bezmialem Vakif University, 34093 Fatih, İstanbul, Turkey
[c] Department of Organic Agriculture Management, Pamukkale University, Denizli, Turkey
[d] Department of Biotechnology, Faculty of Science, Bartin University, 74110 Bartin, Turkey
[e] Department of Chemistry, Science & Arts College, Rabigh Branch, King Abdulaziz University, Rabigh 21911, Saudi Arabia
[f] Department of Biology, Faculty of Science, Pamukkale University, 20070 Denizli, Turkey
[g] Department of Chemistry, Faculty of Science, Imam Mohammad Ibn Saud Islamic University (IMSIU), Riyadh 11623, Saudi Arabia
[h] Chemistry Department, Faculty of Science, Islamic University of Madinah, Madinah, 42351, Saudi Arabia
[i] Department of Biological Sciences and Chemistry, College of Arts and Sciences, University of Nizwa, Nizwa 616, Oman

ARTICLE INFO

Keywords:
Thiosemicarbazones
Cholinesterase inhibitors
Neuroblastoma
Cytotoxicity
Molecular docking

ABSTRACT

A novel series of 4-thiomorpholinophenyl-thiosemicarbazones **(3a–p)** was synthesized and characterized by spectroscopic techniques. The compounds were evaluated for inhibitory activity against acetylcholinesterase (AChE) and butyrylcholinesterase (BChE), key enzymes associated with neurodegenerative disorders. All derivatives exhibited potent inhibition, with nanomolar IC_{50} values ranging from 11.36 to 34.17 nM (AChE) and 33.42 to 79.77 nM (BChE), comparable to standard drugs galantamine and tacrine. Compound **3l**, bearing a benzyl group, showed the strongest dual inhibition (AChE IC_{50} = 11.36 nM) and compound **3n** exhibited the highest BChE selectivity (K_i = 33.42 ± 2.38 nM). Anticancer activity was assessed against SH-SY5Y neuroblastoma and HEK-293 cell lines. Compound **3l** demonstrated selective cytotoxicity against SH-SY5Y cells (IC_{50} = 21.11 ± 0.42 μM) with minimal toxicity toward HEK-293 cells (IC_{50} = 69.49 ± 4.27 μM, SI = 3.3), comparable to sorafenib. Molecular docking showed multiple π–π and hydrogen-bond interactions of **3l** with AChE (Tyr-72, Tyr-337, Trp-286, His-447, Phe-295, Tyr-124) and **3n** with BChE (Trp-231, Phe-329, Pro-285, Gln-119, Thr-120). MM-GBSA calculations indicated favorable binding energies (−70.74 and − 67.09 kcal/mol) driven by van der Waals and lipophilic forces. Molecular dynamics simulations confirmed stable complexes with RMSD ~1.4 Å for ligands, ~2.0 Å for proteins, persistent interactions, and reduced flexibility (RMSF ~1.5 Å). ADME analysis suggested acceptable drug-like properties. These results highlight **3l** and **3n** as promising scaffolds for dual cholinesterase inhibition and selective anticancer activity.

1. Introduction

Alzheimer's disease (AD), the most prevalent type of dementia, affects 60–70 % of cases globally. It is a progressive neurodegenerative disorder marked by cognitive decline, memory loss, disorientation, and behavioral changes, which substantially impact daily functioning [1]. Key neuropathological features include extracellular amyloid-β plaques, intracellular tau neurofibrillary tangles, and widespread neuronal and synaptic loss, mitochondrial dysfunction [2,3], especially in the hippocampus and cortex. Although its exact cause is unclear, oxidative stress, inflammation, and neurotransmitter imbalances contribute to AD pathogenesis [4–9].

Currently approved AD drugs, including acetylcholinesterase (AChE) inhibitors (donepezil, rivastigmine, galantamine) and the NMDA (*N*-methyl-D-aspartate receptor) receptor antagonist memantine, provide only symptomatic relief without halting disease progression. AChE inhibitors are widely used in mild to moderate AD based on the cholinergic hypothesis, which links cognitive decline to cholinergic neuron loss in

* Corresponding authors.
E-mail addresses: smgomha@iu.edu.sa (S.M. Gomha), hsenol@bezmialem.edu.tr (H. Şenol).

https://doi.org/10.1016/j.bioorg.2025.109364
Received 27 September 2025; Received in revised form 29 November 2025; Accepted 8 December 2025
Available online 9 December 2025

the basal forebrain [10–14].

Acetylcholinesterase (AChE) and butyrylcholinesterase (BChE) are crucial enzymes that hydrolyze the neurotransmitter acetylcholine (ACh) in the central nervous system. In the early stages of AD, AChE activity predominates, whereas BChE activity increases as the disease progresses, indicating the therapeutic relevance of dual AChE/BChE inhibition. Therefore, the development of selective or dual cholinesterase inhibitors has become a crucial pharmacological strategy to enhance cholinergic signaling, improve synaptic function, and potentially slow cognitive deterioration in AD patients [15–20].

Interestingly, the concept of cholinesterase inhibition extends beyond neurodegenerative diseases and has shown relevance in certain cancers, including neuroblastoma. Neuroblastoma is a pediatric extracranial solid tumor initiating from neural crest cells, primarily affecting children under the age of five. It exhibits a heterogeneous clinical course ranging from spontaneous regression to aggressive progression with poor prognosis. Current treatments for high-risk neuroblastoma, such as chemotherapy, surgery, radiation, and immunotherapy, often result in significant toxicity and long-term side effects [21–26]. Thus, there is a evolving interest in identifying compounds that exhibit both anti-neuroblastoma activity and neuroprotective potential [27,28].

Cholinesterases have been implicated in cancer cell proliferation, differentiation, and apoptosis, with emerging evidence suggesting their role in tumor progression and drug resistance. Several studies have demonstrated that AChE and BChE are differentially expressed in certain tumor types, including neuroblastoma, and may serve as potential therapeutic targets [14,29–31]. As such, compounds with cholinesterase inhibitory activity could exert cytotoxic effects on neuroblastoma cells, offering a dual therapeutic approach for both neurodegenerative and oncological indications [32,33].

Thiosemicarbazones are a class of Schiff base derivatives recognized for their various biological activities, including antimicrobial, antiviral, antitumor [34], and enzyme inhibitory properties against diverse targets [35–41]. Their pharmacological versatility is largely attributed to their metal-chelating capacity, structural flexibility, and their interactions with various biological targets. Several thiosemicarbazone derivatives have been reported to inhibit cholinesterase enzymes and induce cytotoxic effects in different cancer cell lines, making them promising candidates for multitarget drug development [35,42–50] (Fig. 1) Incorporation of heterocyclic moieties such as morpholine and thiomorpholine into the thiosemicarbazone scaffold has been explored to improve pharmacokinetic and pharmacodynamic properties. Morpholine derivatives, due to their moderate polarity, favorable solubility, and capacity to form hydrogen bonds, are widely utilized in drug design to enhance bioavailability and metabolic stability [51–56]. Similarly, thiomorpholine, a sulfur-containing analog of morpholine, offers additional potential due to the presence of a softer sulfur atom that may enhance lipophilicity and increase interactions with hydrophobic regions of target proteins. Moreover, the presence of sulfur in thiomorpholine can facilitate alternative binding modes via sulfur-mediated interactions, potentially improving binding affinity and selectivity toward enzymatic or cellular targets [57–59]. Thus, the integration of morpholine and particularly thiomorpholine rings into thiosemicarbazone frameworks represents a promising modification to modulate biological activity, improve membrane permeability, and enhance multi-target engagement in both enzyme inhibition and anticancer applications.

In this context, we report the synthesis and comprehensive evaluation of a novel series of 4-thiomorpholinophenyl-thiosemicarbazone **3a–p** derivatives. These compounds were characterized by NMR, HRMS and IR spectroscopic methods and evaluated for their inhibitory activities against AChE and BChE, as well as their cytotoxic effects on SH-SY5Y human neuroblastoma and Human Embryonic Kidney 293 (HEK-293) cells. In addition, molecular docking and molecular dynamics simulations were performed to elucidate the binding interactions and structural stability of the ligand-protein complexes.

2. Results and discussions

2.1. Chemistry

The targeted compounds **3a–p** was synthesized via the condensation reaction of 4-thiomorpholinobenzaldehyde **(1)** with various substituted thiosemicarbazides **2a–p** in methanol under reflux for 4–6 h with catalytic amount of acetic acid, as depicted in Scheme 1. The successful synthesis of 4-thiomorpholinophenyl-thiosemicarbazone derivatives **3a–p** was confirmed by detailed analysis of their ^{1}H and ^{13}C NMR spectral data. In the ^{1}H NMR spectra of representative compounds, the appearance of two distinct singlets corresponding to NH-protons in the range of 11.23–11.90 ppm and 8.86–10.30 ppm, along with a singlet at 7.90–8.06 ppm attributed to azomethine (-CH=N-) proton, confirms the successful condensation of thiosemicarbazide with the aldehydic group.

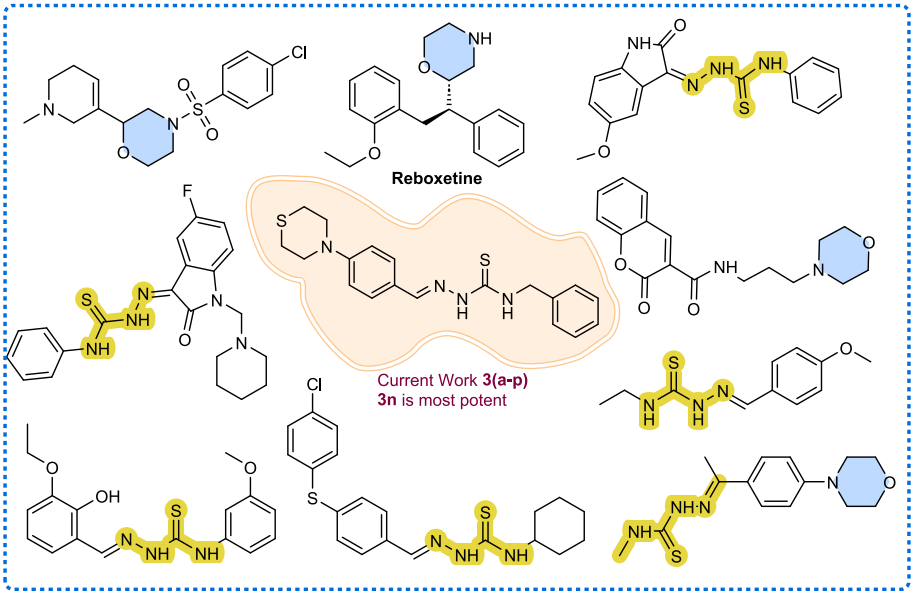

Fig. 1. Reported compounds as Anti-Alzheimer's agents having thiosemicarbazone and sulfonyl moieties [60–68]

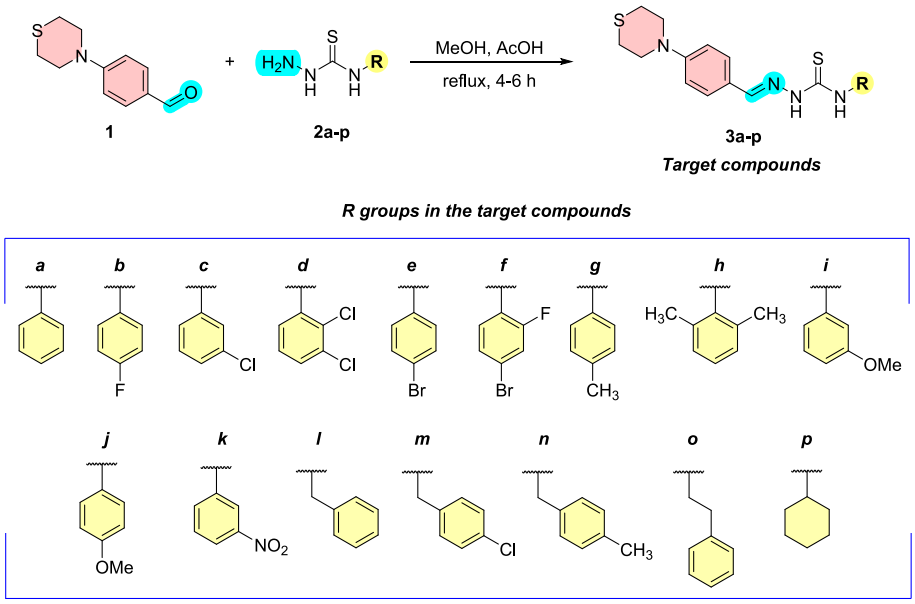

Scheme 1. Synthesis of **3a–p** via condensation of 4-thiomorpholinobenzaldehyde and thiosemicarbazides.

Additionally, signals observed in the aliphatic region (2.53–3.85 ppm) are consistent with methylene (-CH_2-) protons of thiomorpholine ring.

The ^{13}C NMR spectra further support the structural assignment, displaying characteristic downfield signals in the range of δ 177.62–175.63 ppm for the thiocarbonyl carbon (C=S) and δ 160.31–137.7 ppm for the imine carbon (C=N), confirming the formation of the thiosemicarbazide moiety.

2.2. Cholinesterase inhibition studies

To assess the cholinesterase inhibitory potential of the synthesized compounds **(3a–p),** their in-vitro inhibitory activities against AChE and BChE were evaluated using a modified Ellman's method. IC_{50} values determined for both enzymes, alongside inhibition constants (K_i) calculated from kinetic data to provide a more precise measurement of enzyme-ligand binding affinity. The correlation coefficients (R [2]) indicate the goodness of fit for the kinetic data to the applied inhibition models. Reference drugs galantamine and tacrine were also tested under identical conditions for comparative purposes. The results are summarized in Table 1.

The cholinesterase inhibition data presented in Table 1 demonstrate that the synthesized 4-thiomorpholinophenyl-thiosemicarbazone derivatives **3a–p** exhibit a wide range of inhibitory activities against both AChE and BChE with several compounds outperforming the reference

Table 1
IC_{50} and K_i values of synthesized **3a–p** compounds against AChE and BChE.

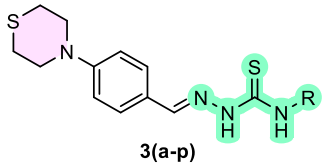

Compounds	R group	IC_{50} (nM)*				K_i (nM)	
		AChE	r^2	BChE	r^2	AChE	BChE
3a	Phenyl	18.74 ± 2.26	0.938	72.65 ± 6.69	0.932	14.76 ± 1.26	59.27 ± 4.78
3b	4-fluorophenyl	23.70 ± 1.22	0.949	79.77 ± 7.11	0.947	21.25 ± 2.54	53.87 ± 5.62
3c	3-chlorophenyl	20.61 ± 1.39	0.943	65.64 ± 6.33	0.976	16.15 ± 0.92	54.18 ± 8.64
3d	2,3-dichlorophenyl	16.82 ± 2.21	0.917	44.30 ± 5.19	0.973	12.76 ± 0.98	36.14 ± 5.04
3e	4-bromophenyl	30.26 ± 2.10	0.933	76.41 ± 6.43	0.943	24.34 ± 2.35	68.74 ± 6.01
3f	4-bromo-2-fluorophenyl	17.26 ± 0.96	0.966	46.16 ± 5.88	0.928	14.31 ± 1.07	39.27 ± 4.48
3g	4-methylphenyl	19.53 ± 1.33	0.940	52.78 ± 5.16	0.995	17.71 ± 2.93	39.17 ± 4.58
3h	2,6-dimethylphenyl	19.43 ± 2.52	0.963	69.23 ± 4.48	0.975	15.42 ± 1.08	57.11 ± 7.26
3i	3-methoxyphenyl	34.17 ± 2.01	0.927	76.06 ± 4.99	0.946	30.52 ± 3.16	65.08 ± 9.06
3j	4-methoxyphenyl	22.21 ± 3.16	0.946	58.44 ± 6.13	0.972	18.57 ± 2.14	51.32 ± 4.67
3k	3-nitrophenyl	23.71 ± 2.25	0.914	69.73 ± 6.42	0.954	20.63 ± 1.45	60.82 ± 3.57
3l	**Benzyl**	11.36 ± 0.98	0.947	40.45 ± 7.38	0.922	**11.15 ± 0.75**	35.80 ± 3.87
3m	4-chlorobenzyl	28.55 ± 3.42	0.918	66.81 ± 7.21	0.966	22.68 ± 1.25	61.84 ± 5.38
3n	**4-methylbenzyl**	12.81 ± 1.31	0.951	44.54 ± 4.13	0.925	11.25 ± 1.18	**33.42 ± 2.38**
3o	Phenethyl	19.41 ± 3.61	0.990	59.21 ± 5.11	0.948	15.24 ± 1.82	52.76 ± 8.28
3p	Cyclohexyl	18.90 ± 2.54	0.957	56.32 ± 3.89	0.954	15.28 ± 1.07	51.07 ± 6.74
Galantamine	Reference drug	33.85 ± 3.79	0.957	68.07 ± 6.81	0.989	25.87 ± 3.68	58.71 ± 6.37
Tacrine	Reference drug	66.73 ± 4.94	0.951	78.73 ± 6.56	0.963	50.27 ± 4.06	63.90 ± 5.75

* Inhibition assays for each compound were performed in triplicate ($n = 3$), and the reported values represent the mean of these measurements.

drugs galantamine and tacrine. In general, most compounds showed stronger inhibition of AChE than BChE, suggesting a degree of selectivity, although some derivatives demonstrated potent dual inhibition profiles. Notably, compound **3l** (benzyl) exhibited the lowest IC_{50} for AChE (11.36 nM) and one of the best K_i values (11.15 ± 0.75 nM), indicating high binding affinity and strong interface with the enzyme active site. This compound also showed noteworthy BChE inhibition, suggesting a favorable dual inhibitory profile. Alkyl-substituted compound **3n** (4-methylbenzyl) exhibited the lowest K_i value against BChE (33.42 ± 2.38 nM) among all synthesized derivatives, highlighting its strong binding affinity and potent inhibitory effect on BChE. Alkyl-substituted other compounds also displayed remarkable inhibition, further supporting the idea that bulky or hydrophobic moieties contribute positively to activity.

Halogenated derivatives, such as **3d** (2,3-dichlorophenyl), also demonstrated strong dual enzyme inhibition, with low nanomolar IC_{50} and K_i values, highlighting the role of electron-withdrawing substituents in improving binding affinity, likely due to favorable hydrophobic and π–π stacking interactions within the enzyme gorge. In contrast, methoxy-substituted derivatives like **3i** (3-methoxyphenyl) and **3j** (4-methoxyphenyl) showed moderate activity, with slightly higher IC_{50} values compared to halogenated or benzyl-containing analogs.

Interestingly, some non-aromatic or partially aromatic compounds such as **3o** (phenethyl) and **3p** (cyclohexyl) showed moderate inhibition, suggesting that full aromaticity may enhance π-π interactions with key residues within the cholinesterase active site. The correlation coefficients (R [2]) for all data ranged from 0.91 to 0.99, confirming the robustness and reliability of the kinetic analyses and dose-response modeling. Overall, the benzyl-containing derivative **3l** and the 4-methylbenzyl-substituted compound **3n** emerged as the most promising inhibitors in the series, exhibiting the lowest K_i values for AChE and BChE, respectively. They are highlighting the critical role of benzyl and alkyl benzyl groups in enhancing enzyme binding through hydrophobic interactions.

2.3. Cytotoxicity studies

To assess the anticancer potential of the synthesized 4-thiomorpholinophenyl-thiosemicarbazone derivatives **3a–p,** their cytotoxic effects were evaluated against the human neuroblastoma cell line (SH-SY5Y) and the non-cancerous human embryonic kidney cell line (HEK-293) using the crystal violet assay. IC_{50} values (μM) were calculated for both cell lines to determine the concentration required to reduce cell viability by 50 %. In addition, the selectivity index (SI) was determined by dividing the IC_{50} value in HEK-293 cells by that in SH-SY5Y cells (HEK-293/SH-SY5Y), allowing for an estimation of each compound's tumor selectivity. The results are given in Table 2**.**

The cytotoxicity results reveal that most of the tested compounds exhibit moderate to good activity against SH-SY5Y neuroblastoma cells, with varying degrees of selectivity over normal HEK-293 cells. Notably, several compounds demonstrate superior or comparable selectivity indices to the reference drug sorafenib (SI = 3.3), indicating their potential as selective antitumor agents.

The most striking result was observed with compound **3l** (benzyl group), which exhibited an IC_{50} of 21.11 ± 0.42 μM in SH-SY5Y cells, while maintaining low toxicity toward HEK-293 cells (IC_{50} = 69.49 ± 4.27 μM), resulting in the highest selectivity index among all test compounds (SI = 3.3), identical to that of sorafenib. This suggests that **3l** has a highly favorable cytotoxicity profile, combining potent anticancer activity with minimal off-target toxicity.

Compound **3n** (4-methylbenzyl) also demonstrated a high level of selectivity, with an SI of 2.4, due to its strong activity in SH-SY5Y cells (IC_{50} = 34.13 ± 1.36 μM) and relatively low toxicity in HEK-293 cells (IC_{50} = 80.48 ± 5.41 μM). While slightly less selective than **3l**, this compound remains one of the most promising candidates in terms of safety and efficacy.

Table 2
IC_{50} (μM) of 3a–p for HEK-293 and SH-SY5Y cells with corresponding SI.

Compounds	R group	IC_{50} [μM]		Selectivity index
		HEK-293	SH-SY5Y	HEK-293/SH-SY5Y
3a	Phenyl	81.31 ± 6.00	53.88 ± 1.71	1.5
3b	4-fluorophenyl	54.44 ± 2.24	33.49 ± 2.17	1.6
3c	3-chlorophenyl	51.50 ± 3.76	41.41 ± 1.34	1.2
3d	2,3-dichlorophenyl	46.85 ± 1.79	35.56 ± 2.31	1.3
3e	4-bromophenyl	53.64 ± 4.52	28.31 ± 0.85	1.9
3f	4-bromo-2-fluorophenyl	64.07 ± 0.64	34.12 ± 0.91	1.8
3g	4-methylphenyl	47.26 ± 4.02	35.47 ± 2.95	1.3
3h	2,6-dimethylphenyl	60.59 ± 3.28	37.29 ± 2.98	1.6
3i	3-methoxyphenyl	58.55 ± 0.58	40.59 ± 1.23	1.4
3j	4-methoxyphenyl	58.39 ± 2.38	44.88 ± 2.32	1.3
3k	3-nitrophenyl	70.34 ± 1.08	51.63 ± 5.67	1.3
3l	**Benzyl**	**69.49 ± 4.27**	**21.11 ± 0.42**	**3.3**
3m	4-chlorobenzyl	48.36 ± 4.02	37.86 ± 1.76	1.3
3n	**4-methylbenzyl**	**80.48 ± 5.41**	**34.13 ± 1.36**	**2.4**
3o	Phenethyl	53.62 ± 4.27	34.13 ± 1.23	1.5
3p	Cyclohexyl	52.46 ± 1.57	36.52 ± 2.38	1.4
Sorafenib	Reference drug	13.26 ± 0.14	3.92 ± 0.02	**3.3**

Halogenated derivatives such as **3e** (4-bromophenyl) and **3f** (4-bromo-2-fluorophenyl) also displayed relatively high SI values (1.7–1.9), indicating a favorable selectivity trend among bromine-containing analogs. These findings suggest that electron-withdrawing halogen substituents may contribute to increased cytotoxicity in tumor cells, possibly via enhanced membrane permeability or increased interactions with intracellular targets.

This reduced selectivity may be due to higher polarity or steric hindrance from the methoxy groups, limiting differential uptake or targeting. Most other compounds exhibited intermediate SI values ranging from 1.2 to 1.6, including **3b, 3h, 3o,** and **3p**, which indicates a moderate level of tumor preference but room for structural optimization. Notably, while compound **3b** had a decent SI of 1.6, its moderate IC_{50} in SH-SY5Y (33.49 μM) makes it a viable scaffold for further derivatization.

Overall, compounds **3l** and **3n** emerged as the most favorable candidates due to their combination of low IC_{50} values in neuroblastoma cells and favorable selectivity indices. These results support the hypothesis that specific benzyl substituents may enhance selective cytotoxicity toward cancer cells while tumbling harm to healthy cells.

Furthermore, to strengthen the SAR interpretation beyond hydrophobic contributions, molecular orbital distribution and electrostatic potential mapping were considered. Compounds **3l** and **3n**, which showed the lowest K_i values, displayed greater HOMO density localized on the benzyl/alkyl-benzyl aromatic system, supporting more efficient π–π donor interactions with Trp/Tyr residues in the active gorge. In contrast, methoxy-substituted analogs, which exhibited weaker activity, displayed more polarized electron density and increased steric bulk, reducing optimal aromatic stacking geometry. Halogenated derivatives

such as **3d** benefited from strong electron-withdrawing substituents, increasing lipophilic surface area and enhancing halogen-bond-supported anchoring within the enzyme cleft (Fig. 2).

2.4. Molecular docking studies

In this study, induced fit docking (IFD) and Molecular Mechanics Generalized Born Surface Area (MM-GBSA) ΔG binding free energy calculations were performed to evaluate the binding affinities and interaction profiles of the most active synthesized compounds **(3l** and **3n)** against AChE and BChE enzymes. Tacrine, a well-known cholinesterase inhibitor, was included as a reference drug to benchmark the docking and binding energy results. The IFD scores and detailed MM-GBSA energy decomposition analysis results are given in Table 3**.**

Table 3 summarizes the IFD docking scores and MM-GBSA energy components for compounds **3l, 3n,** and **tacrine** with AChE and BChE enzymes. Both compounds **3l** and **3n** demonstrate superior IFD docking scores compared to tacrine, especially notable in the case of **3l** with AChE (−10.686 kcal/mol vs. -10.575 kcal/mol) and **3n** with BChE (−9.077 kcal/mol vs. -7.501 kcal/mol). This suggests a stronger predicted binding affinity for these novel compounds. The MM-GBSA binding free energy (ΔG Bind) calculations further reinforce these observations, with **3l** and **3n** exhibiting significantly more favorable binding energies than tacrine for both enzymes. For instance, **3l-AChE** shows a ΔG Bind of −70.74 kcal/mol, substantially better than tacrine-AChE's − 54.29 kcal/mol, indicating a more stable complex formation. Breaking down the energy components reveals that van der Waals (vdW) and lipophilic (Lipo) interactions are major contributors to the enhanced binding of **3l** and **3n**. Specifically, the vdW energies for **3l** and **3n** complexes are approximately −59 kcal/mol, almost double the vdW contribution of tacrine complexes (∼ −31 kcal/mol), emphasizing strong hydrophobic contacts. Conversely, the Coulomb (electrostatic) interaction terms show unfavorable positive values for tacrine with AChE and especially BChE, suggesting less favorable electrostatic complementarity. In contrast, **3l** and **3n** present negative Coulomb contributions, indicating stronger electrostatic interactions with the enzyme active sites. Other energy terms such as covalent, hydrogen bonding, and solvation energies vary but appear less impactful relative to the dominant vdW and lipophilic forces.

Overall, the computational analysis strongly suggests that compounds **3l** and **3n** have higher predicted binding affinities and more favorable interaction profiles than tacrine with both AChE and BChE, highlighting their potential as potent cholinesterase inhibitors.

Fig. 3 shows the 2D and 3D ligand–protein interactions and binding modes of the **3l–AChE** and **3n–BChE** complexes.

In Fig. 3a, the 2D interaction map of the **3l–AChE** complex reveals a highly interactive binding profile dominated by hydrogen bonding and aromatic π–π stacking. The sulfur atom of the thiosemicarbazide moiety forms a hydrogen bond with Phe-295, while the terminal amino group interacts with Tyr-124. These polar interactions help stabilize the

Table 3
IFD docking and MM-GBSA energy decomposition analysis of the most active compounds versus tacrine.

Docking and MM-GBSA ΔG parameters (kcal/Mol)	3l-AChE	3n-BChE	Tacrine-AChE	Tacrine-BChE
Induced fit docking (IFD) score	−10.686	−9.077	−10.575	−7.501
Binding free energy	−70.74	−67.09	−54.29	−58.29
Coulomb (electrostatic) contribution	−14.57	−19.20	8.42	42.45
Covalent interaction energy	5.38	9.04	1.96	2.21
Hydrogen bond contribution	−0.44	−0.92	−0.51	−0.74
Lipophilic interaction contribution	−36.07	−30.54	−16.82	−14.65
Solvation energy (GB model)	42.70	37.18	−9.69	−48.54
Van der Waals interaction contribution	−58.98	−58.88	−31.04	−30.96

molecule at the entrance of the active site. However, the most remarkable feature is the presence of five *pi-pi* stacking interactions. The benzylidene ring participates in two stacking interfaces with Tyr-337 and His-447, and the benzyl ring engages in three stacking contacts with Tyr-72 and Trp-286. The extensive π-system of compound **3l** enables it to align perfectly with aromatic residues deep within the AChE gorge, stabilizing the complex through cumulative non-covalent forces. Fig. 3b**,** which shows the 3D binding mode of **3l** in AChE, further supports this observation. The hydrogen bonds (yellow dashed-lines) and π–π stacking interactions (turquoise dashed-lines) are well distributed across the binding pocket. The π–π stacking distances range from 4.14 to 5.31 Å, indicating optimal spacing for aromatic overlap. The binding surface analysis shows near-complete overlap between the ligand (blue cloud) and the protein pocket (grey cloud), suggesting an excellent steric and electronic complementarity. Only a small portion of the benzyl ring is slightly solvent-exposed, indicating deep insertion into the active site.

In Fig. 3c, the 2D ligand–protein interaction diagram of the **3n–BChE** complex shows a slightly different binding profile. Although compound **3n** engages in fewer π–π stacking interactions than **3o**, it compensates through strong hydrogen bonding and focused aromatic contacts. The nitrogen atoms of the thiosemicarbazide moiety form hydrogen bonds with Pro-285 and Gln-119, while the sulfur atom interacts with Thr-120. The 4-methylbenzyl ring establishes two π–π stacking interactions with Trp-231, and the benzylidene ring stacks once with Phe-329. Although fewer in number, these stacking interactions are formed with strategically important residues, likely stabilizing the ligand in the mid-gorge region of BChE. Fig. 3d, presenting the 3D LPI of the **3n–BChE** complex, confirms tight binding with complete overlap of ligand and protein surfaces. The hydrogen bond lengths (2.49–2.70 Å) and π–π stacking distances (4.17–5.49 Å) fall within favorable ranges.

In conclusion, compound **3l** showed strong AChE inhibition through multiple π–π interactions with Tyr-337, His-447, Tyr-72, and Trp-286, and hydrogen bonds with Phe-295 and Tyr-124. Its deep binding within the active site explains its high affinity. Compound **3n**, on the

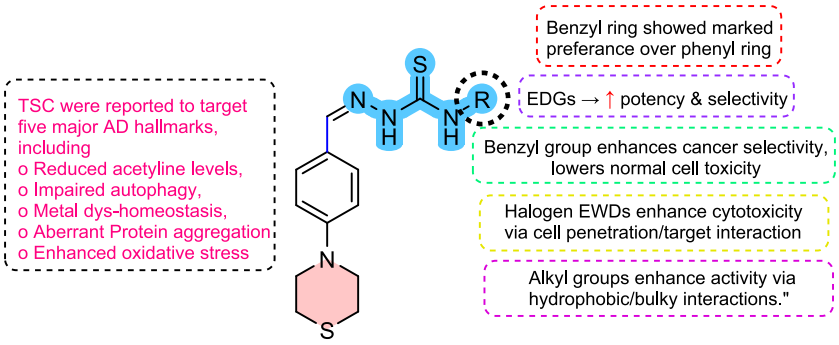

Fig. 2. Representation of structural diversity and its influence on biological activity through chemical modifications.

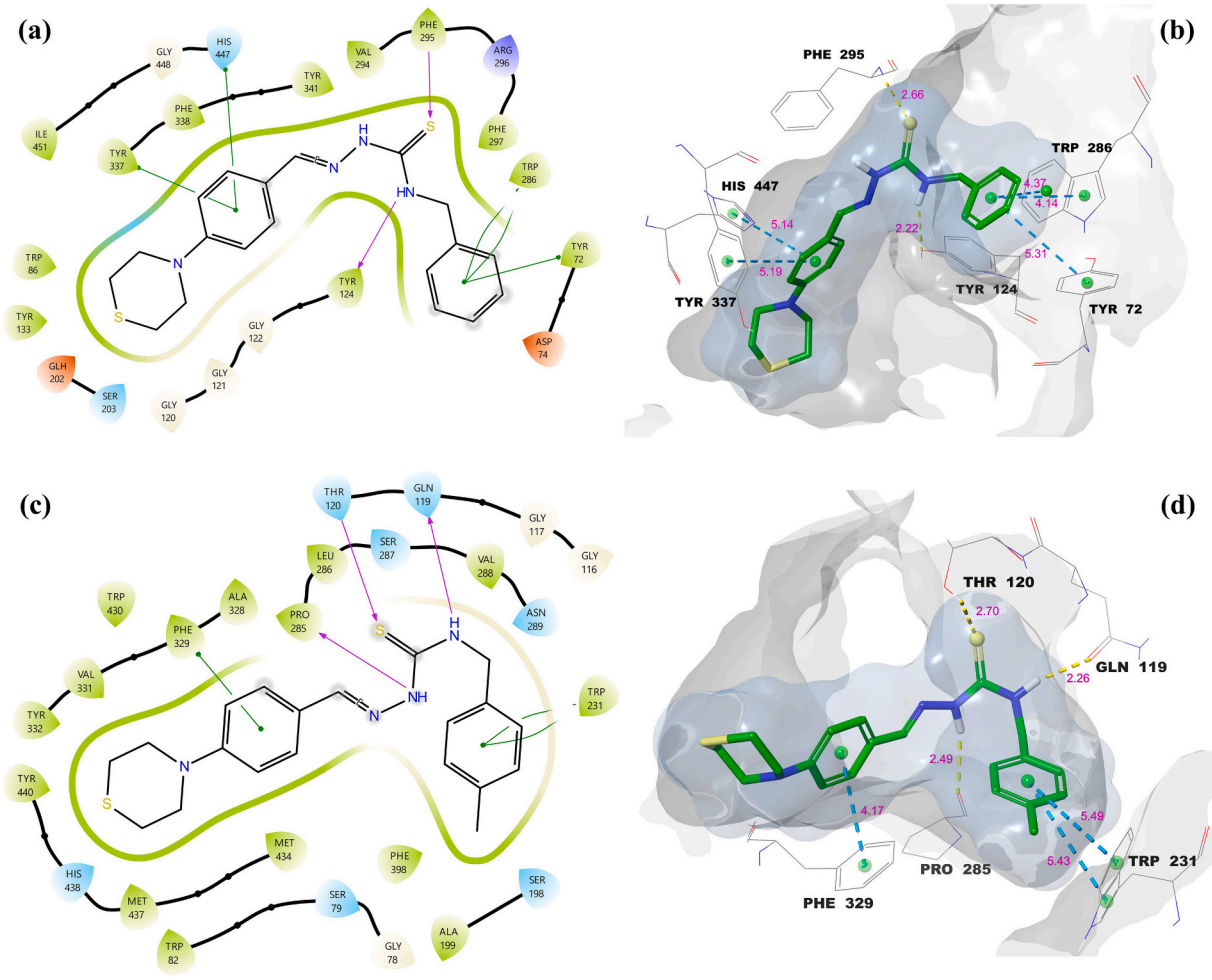

Fig. 3. Molecular docking-based ligand–protein interaction diagrams and binding modes of selected complexes: (a) 2D interaction of **3l** with AChE, (b) 3D binding pose of **3l** in AChE active site, (c) 2D interaction of **3n** with BChE, (d) 3D binding pose of **3n** in BChE active site.

other hand, formed hydrogen bonds with Pro-285, Gln-119, and Thr-120, and π–π interactions with Trp-231 and Phe-329 in BChE, supporting its selectivity.

2.5. Molecular dynamics simulations

Molecular dynamics simulations were conducted on **3l–AChE** and **3n–BChE** complexes for 100 ns. The molecular dynamics simulation analysis of **3l–AChE** complex is given in Fig. 4.

Fig. 4a illustrates the percentage distribution of 2D interactions between the ligand and amino acid residues. The benzyl moiety of the ligand engages in multiple π–π stacking interactions with Tyr-124 (during 38 % of simulation time), Trp-286 (28 % of sim.), and Phe-297 (29 % of sim.). Additional π–π interactions are observed between the phenyl ring attached to the thiomorpholine moiety and residues Trp-86 (14 % of sim.) and Tyr-337 (12 % of sim.). Moreover, Tyr-124 forms a hydrogen bond with the thiosemicarbazide group. Lastly, the thiosemicarbazide moiety also interacts with Phe-295 through a water-mediated hydrogen bond. Fig. 4b represents the RMSD (Root Mean Square Deviation) values of protein Cα (pale blue), ligand atoms fit on protein (red) and ligand's(pink). As observed, the ligand atoms exhibit an RMSD of approximately 1.4 Å, whereas the protein Cα atoms show a value around 2.2 Å. The average RMSD of the ligand relative to the protein is approximately 2.5 Å. Fig. 4c illustrates the fluctuations of the protein Cα atoms throughout the simulation. The green lines indicate the amino acid residues involved in interactions with the ligand. As observed, although the average RMSF (Root Mean Square Fluctuation) of the protein is around 1.5 Å, the residues interacting with the ligand exhibit lower fluctuations compared to the other residues. Fig. 4d presents the amino acid residues that interact with the ligand throughout the simulation, along with the types of interactions involved. Green lines represent hydrogen bonds, blue indicates water-bridged hydrogen bonds, and purple denotes hydrophobic interactions. As shown, Tyr-124 exhibits the highest interaction percentage at 120 %, indicating that it engages with the ligand through multiple interaction modes simultaneously, namely, hydrophobic contacts and hydrogen bonding, with different regions of the ligand. This elevated percentage suggests persistent and overlapping interactions throughout the simulation. In addition, notable hydrophobic interactions are also observed with Trp-86, Trp289, Phe-297, Tyr-337, and Tyr-341. Overall, the results depicted in Fig. 4 comprehensively illustrate the stability and interaction profile of the ligand–protein complex during the simulation. The ligand demonstrates consistent binding behavior, supported by low RMSD values and strong, persistent interactions with key residues such as Tyr-124. The reduced flexibility (RMSF) of interacting residues further indicates a stabilizing effect of the ligand within the binding pocket. Collectively, these findings highlight the ligand's favorable binding characteristics and its potential as a stable and effective inhibitor.

The molecular dynamics simulation analysis of **3n–BChE** complex is given in Fig. 5. Fig. 5a illustrates the percentage distribution of 2D interactions between the ligand and amino acid residues. The thiosemicarbazide functionality provides various hydrogen and water-bridged hydrogen bond interactions. Water-bridged hydrogen bond interactions were observed with Asn-289 (14 % of sim.) and Asp-70 (25 %

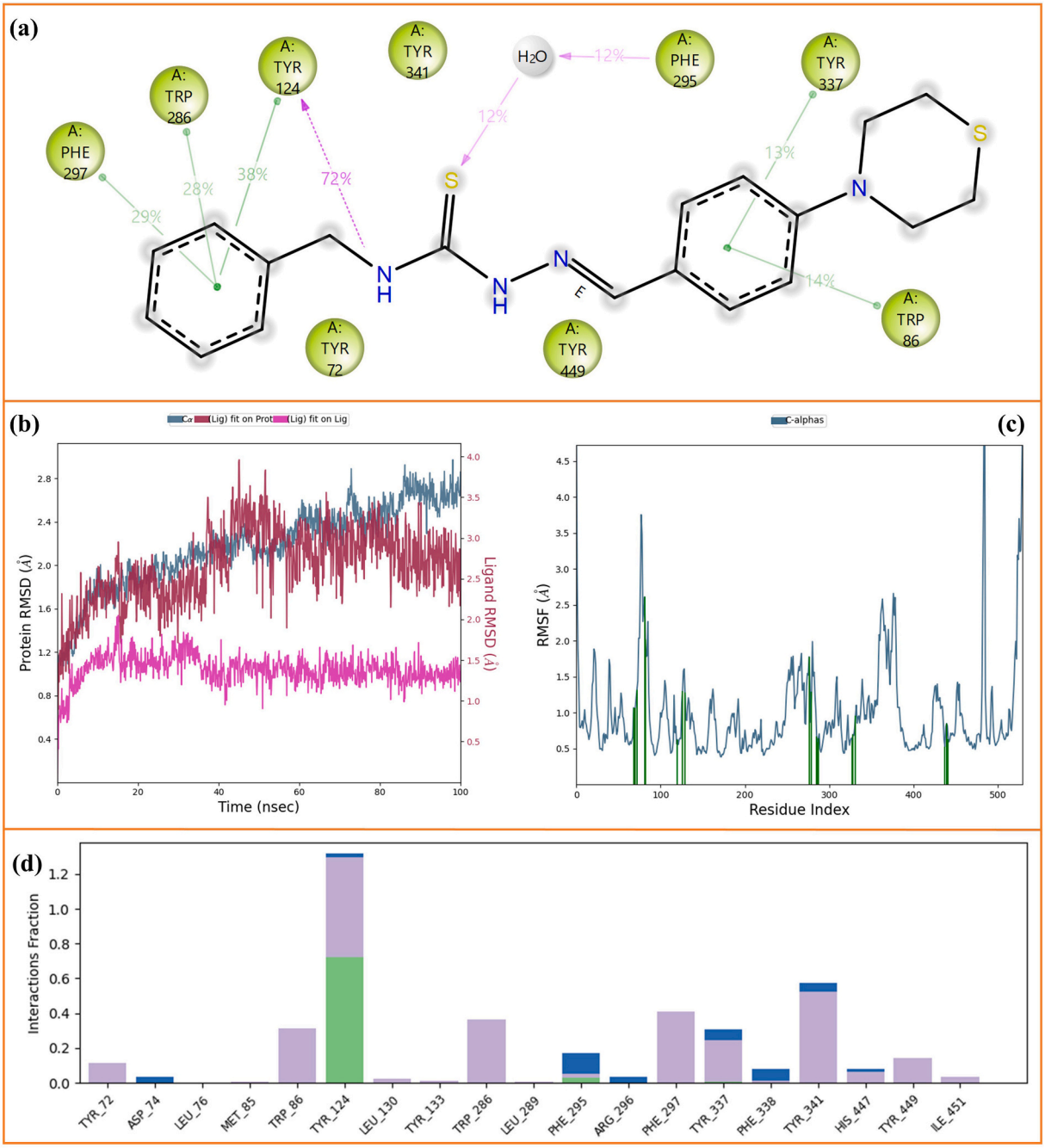

Fig. 4. MD analysis of **3l–AChE**: (a) 2D ligand–residue interactions, (b) RMSD of protein Cα and ligand, (c) RMSF of protein residues, (d) interaction histogram.

of sim.), while a direct hydrogen bond was formed with Ser-287 (16 % of sim.). Additionally, the phenyl rings of the ligand formed π-π stacking interactions with Phe-329 (43 % of sim.) and Phe-73 (44 % of sim.), further contributing to the stability of the ligand–protein complex.

Fig. 5b displays the RMSD plots. As observed, the ligand maintains an RMSD of approximately 1.4 Å, while the protein Cα atoms exhibit an RMSD around 2.0 Å. The RMSD of the ligand fit on the protein increases to approximately 2.4 Å by 35 ns and subsequently rises to an average of 4.6 Å for the remainder of the simulation. Fig. 5c illustrates the fluctuations of the protein Cα atoms throughout the simulation, with an average RMSF of approximately 1.4 Å. Notably, some of the residues interacting with the ligand are located within regions of higher flexibility, which likely contributes to the elevated ligand RMSD values observed in Fig. 5b. Fig. 5d represents the fractional interaction histogram. As shown, hydrophobic interactions are predominant throughout the simulation. In particular, residues Phe-73, Trp-82, Trp-231, Val-288, and Phe-329 play major roles in these hydrophobic contacts. On the other hand, water-bridged hydrogen bond interactions are also observed with Asn-68, Asp-70, and Asn-289.

Overall, the molecular dynamics simulation results demonstrate that the **3n–BChE** complex exhibits a relatively stable binding profile, supported by low RMSD values and persistent non-covalent interactions. The dominance of hydrophobic interactions, along with key hydrogen and water-bridged hydrogen bonds, particularly involving residues such as Phe-73, Phe-329, Asp-70, and Asn-289, contributes significantly to the ligand's stable association within the active site. Moreover, the increased flexibility of certain interacting residues correlates with the observed ligand mobility, highlighting dynamic adaptability within the binding pocket. These findings suggest that compound **3n** maintains favorable and sustained interactions with BChE, reinforcing its potential

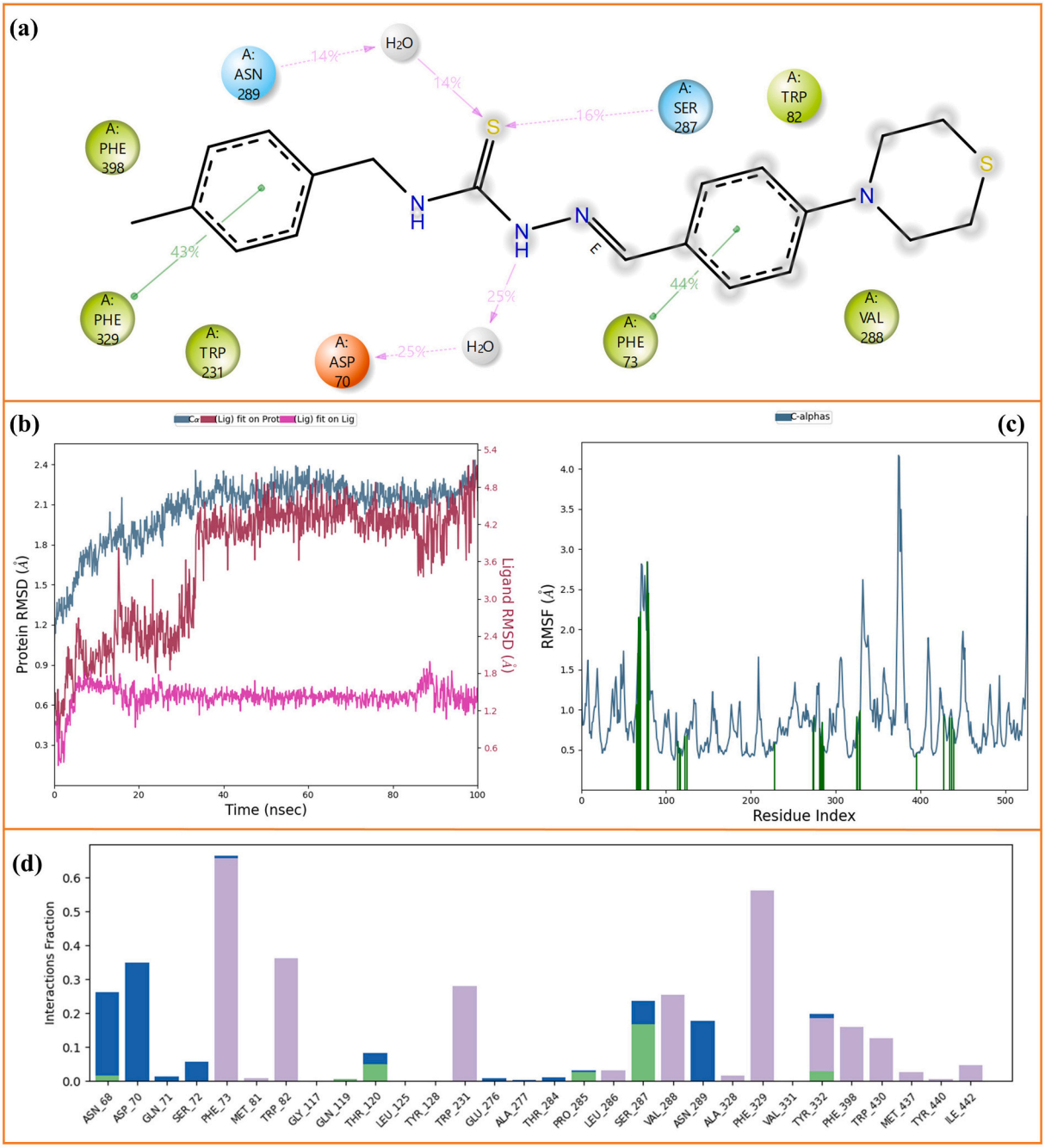

Fig. 5. MD analysis of **3n–BChE:** (a) 2D ligand–residue interactions, (b) RMSD of protein Cα and ligand, (c) RMSF of protein residues, (d) interaction histogram.

as an effective inhibitor candidate.

2.6. Docking validation

Redocking validation was conducted using the co-crystallized ligands of both proteins, where the original co-crystal poses were visualized in green, and the redocked conformations were rendered in magenta (Fig. 6). For AChE (PDB ID: 4EY7, ligand: Donepezil), the redocked pose aligned almost perfectly with the crystallographic conformation, yielding an RMSD of **0.1492 Å**, while for BChE (PDB ID: 6ESJ, ligand: Propidium), an RMSD of **0.8093 Å** was obtained.

Considering that RMSD values below 2.0 Å are widely accepted as an indication of a reliable and well-reproduced docking protocol, the obtained sub-angstrom deviations, especially the 0.15 Å alignment in AChE, reflect excellent structural overlap and high docking accuracy [69]. These results confirm that the docking settings used in this study are robust, reproducible, and suitable for further ligand evaluation.

3. Conclusion

This study reports the successful synthesis and characterization (IR, ^{1}H and ^{13}C NMR) of a new series of 4-thiomorpholinophenyl-thiosemicarbazones **(3a–p)** for lead discovery. All derivatives exhibited several degrees of inhibition ranging between 11.36 and 34.17 nM (AChE) and between 40.45 and 79.77 nM (BChE) as compared to standard drugs galantamine (IC50 values of 33.85 and 68.07) and tacrine (IC50 values of 66.73 and 78.73 nM, respectively). Compound **3l** exhibited the lowest IC_{50} for AChE (11.36 nM) has a benzyl substitution, indicating high binding affinity and solid interaction with the enzyme active site. This compound also showed significant BChE inhibition, suggesting a

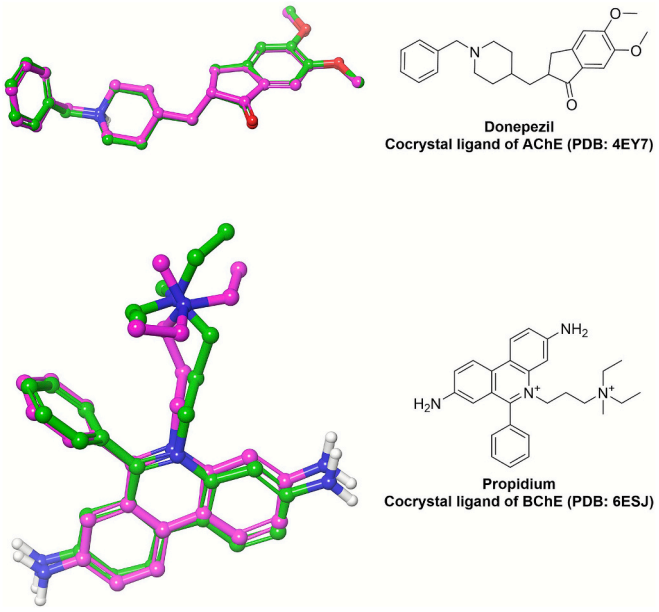

Fig. 6. Molecular docking validation images of related ligands.

favorable dual inhibitory profile. Compound **3n** exhibited the lowest K_i value against BChE (33.42 ± 2.38 nM) among all synthesized derivatives, with alkyl substituent, highlighting its strong binding affinity and potent inhibitory effect on BChE. Additionally, the anticancer activity of 4-thiomorpholinophenyl-thiosemicarbazines **(3a–p)** was evaluated using crystal violet assay against **SH-SY5Y** and **HEK-293** cell lines. IC_{50} values and selectivity indices were calculated to assess cytotoxicity and tumor selectivity. Compound **3 l** (with a benzyl group) showed the most promising results, displaying strong cytotoxicity against SH-SY5Y cells (IC_{50} of 21.11 ± 0.42 μM) and low toxicity toward HEK-293 cells (IC_{50} = 69.49 ± 4.27 μM), yielding the highest selectivity index among all test compounds (SI = 3.3), comparable to sorafenib. This highlights its potent and selective anti-cancer potential.

Molecular docking and molecular dynamics simulations further elucidated the binding mechanisms underlying the potent cholinesterase inhibition of compounds **3l** and **3n**. Compound **3l** exhibited strong interactions with AChE, forming multiple π–π stacking contacts with Tyr-72, Tyr-337, Trp-286, and His-447, as well as hydrogen bonds with Phe-295 and Tyr-124, consistent with its lowest IC_{50} value (11.36 nM). Similarly, compound **3n** showed selective binding to BChE, engaging in π–π interactions with Trp-231 and Phe-329, and hydrogen bonds with Pro-285, Gln-119, and Thr-120. MM-GBSA calculations indicated more favorable binding free energies for both compounds compared to tacrine, driven largely by van der Waals and lipophilic interactions, while Coulomb contributions also supported strong electrostatic complementarity. Molecular dynamics simulations demonstrated stable ligand-protein complexes, with low RMSD and reduced flexibility (RMSF) of key interacting residues such as Tyr-124, Trp-86, and Phe-297 for **3l–AChE**, and Phe-73, Trp-82, Trp-231, and Phe-329 for **3n–BChE**. These results confirm the persistence of critical hydrogen bonding, water-bridged hydrogen bonding, and hydrophobic contacts throughout the simulation, highlighting the structural basis of dual cholinesterase inhibition and supporting the experimental IC_{50} findings. Molecular dynamics simulations confirmed stable complexes with RMSD ~1.4 Å for ligands, ~2.0 Å for proteins, persistent interactions, and reduced flexibility (RMSF ~1.5 Å). ADME analysis suggested acceptable drug-like properties. These results highlight **3l** and **3n** as promising scaffolds for dual cholinesterase inhibition and selective anticancer activity.

4. Experimental section

4.1. Synthesis and characterization

4-thiomorpholinyl-based thiosemicarbazones were synthesized using commercial available reagents from Sigma-Aldrich and solvents from Merck without further purification. Reaction monitoring was performed by thin-layer chromatography (TLC) on aluminum-backed silica gel plates. ^{1}H and ^{13}C NMR spectra were recorded in DMSO-d_6 at 25 °C on a Bruker Ascend 600 MHz spectrometer. All chemical Shifts are reported in ppm, and *J*-values are expressed in Hz. HRMS (High Resolution Mass Spectrometry) analyses were performed using a Thermo Fischer Scientific Triple Quadrupole Orbitrap instrument.

4.2. Synthesis of Thiosemicarbazones (3a–p)

The desired compounds **3a–p** were synthesized in two steps by previously reported method [34,39] with some modification of using ecofriendly solvent (H_2O). In the first step, thiomorpholine (2 mmol) was reacted with 4-fluorobenzaldehyde (2 mmol) in water at 90 °C for 12 h. K_2CO_3 was used as base. The resulting intermediate 4-thiomorpholinobenzaldehyde was isolated in good yield and used for next step without further purification. In the second step, intermediate was then reacted with substituted thiosemicarbazides **2a-p** in ethanol using acetic acid as a catalyst under reflux for 4 h. The reaction progress was tracked using TLC, and the obtained thiosemicarbazones **3a–p** was filtered and rinsed with ethanol, yielding products in moderate to good amounts.

4.2.1. *(E)-N-(4-Chlorophenyl)-2-(4-thiomorpholinobenzylidene) hydrazine-1-carbothioamide (3a)*

Color: yellow; **Yield:** 90 %; **M.P.:** 208–210 °C; **FT-IR (KBr, cm^{-1}):** 3135 (N—H), 2976, 2827 (C-H), 1593 (C=N), 1263 (C=S), 1059 (C—N); **^{1}H NMR (600 MHz, DMSO-d_6)** *δ* 11.64 (1H, s), 9.97 (1H, s), 8.06 (1H, s), 7.78–7.69 (2H, m), 7.68–7.55 (2H, m), 7.37 (2H, t, *J* 7.8), 7.01–6.87 (2H, m), 3.75–3.62 (4H, m), 2.71–2.58 (4H, m); **^{13}C NMR (150 MHz, DMSO-d_6)** *δ* 175.65, 151.51, 143.91, 139.66, 129.62, 128.47, 126.09, 125.55, 123.78, 115.25, 50.52, 25.50; **ESI-HRMS** calcd. For $C_{18}H_{20}N_4S_2$: 357.1207. Found: 357.1196 $[M + H]^+$.

4.2.2. *(E)-N-Phenyl-2-(4-thiomorpholinobenzylidene)hydrazine-1-carbothioamide (3b)*

Color: yellow; **Yield:** 86 %; **M.P.:** 203–205 °C; **FT-IR (KBr, cm^{-1}):** 3141 (N—H), 2979, 2909 (C-H), 1543 (C=N), 1268 (C=S), 1057 (C—N); **^{1}H NMR (600 MHz, DMSO-d_6)** *δ* 11.66 (1H, s), 9.98 (1H, s), 8.05 (1H, s), 7.72 (2H, d, *J* 8.4), 7.56 (2H, dd, *J* 8.6, 5.0), 7.20 (2H, t, *J* 8.6), 6.94 (2H, d, *J* 8.4), 3.77–3.57 (4H, m), 2.74–2.58 (4H, m); **^{13}C NMR (150 MHz, DMSO-d_6)** *δ* 176.03, 160.81, 159.21, 151.52, 143.99, 136.03, 136.02, 129.62, 128.44, 128.39, 123.77, 115.23, 115.16, 115.01, 50.52, 25.50; **ESI-HRMS** calcd. For $C_{18}H_{19}FN_4S_2$: 375.1113. Found: 375.1102 $[M + H]^+$.

4.2.3. *(E)-N-(3-Chlorophenyl)-2-(4-thiomorpholinobenzylidene) hydrazine-1-carbothioamide (3c)*

Color: yellow; **Yield:** 83 %; **M.P.:** 203–205 °C; **FT-IR (KBr, cm^{-1}):** 3123 (N—H), 2964, 2830 (C-H), 1591 (C=N), 1269 (C=S), 1063 (C—N); **^{1}H NMR (600 MHz, DMSO-d_6)** *δ* 11.77 (1H, s), 10.05 (1H, s), 8.06 (1H, s), 7.80 (1H, t, *J* 2.1), 7.73 (2H, d, *J* 8.6), 7.62 (1H, dd, *J* 7.9, 2.0), 7.39 (1H, t, *J* 8.0), 7.24 (1H, dd, *J* 8.0, 2.1), 6.95 (2H, d, *J* 8.7), 3.85–3.55 (4H, m), 2.80–2.58 (4H, m); **^{13}C NMR (150 MHz, DMSO-d_6)** *δ* 175.40, 151.58, 144.41, 141.17, 132.55, 129.99, 129.74, 125.34, 125.16, 124.37, 123.58, 115.19, 50.49, 25.48; **ESI-HRMS** calcd. For $C_{18}H_{19}ClN_4S_2$: 391.0817. Found: 391.0807 $[M + H]^+$.

4.2.4. *(E)-N-(2,6-dichlorophenyl)-2-(4-thiomorpholinobenzylidene) hydrazine-1-carbothio amide (3d)*

Color: yellow; **Yield:** 79 %; **M.P.:** 175–177 °C; **FT-IR (KBr, cm^{-1}):**

3264 (N—H), 2958, 2835 (C-H), 1574 (C=N), 1285 (C=S), 1078 (C—N), **^{1}H NMR (600 MHz, DMSO-d_6)** δ 11.90 (1H, s), 10.07 (1H, s), 8.06 (1H, s), 7.76 (1H, d, *J* 8.0), 7.69 (2H, d, *J* 8.4), 7.56 (1H, d, *J* 8.1), 7.40 (1H, t, *J* 8.0), 6.95 (2H, d, *J* 8.4), 3.78–3.60 (4H, m), 2.71–2.58 (4H, m); **^{13}C NMR (150 MHz, DMSO-d_6)** δ 176.17, 151.56, 144.27, 139.20, 132.02, 129.58, 128.71, 128.38, 128.01, 123.52, 115.25, 50.47, 25.45. **ESI-HRMS** calcd. For $C_{18}H_{18}Cl_2N_4S_2$: 425.0428. Found: 425.0420 $[M+H]^+$.

4.2.5. (E)-N-phenyl-2-(4-thiomorpholinobenzylidene)hydrazine-1-carbothioamide (3e)

Color: yellow; **Yield:** 83 %; **M.P.:** 204–206 °C; **FT-IR (KBr, cm^{-1}):** 3306 (N—H), 3023, 2826 (C-H), 1593 (C=N), 1261 (C=S), 1002 (C—N), **^{1}H NMR (600 MHz, DMSO-d_6)** δ 11.73 (1H, s), 10.01 (1H, s), 8.06 (1H, s), 7.78–7.67 (2H, m), 7.62–7.57 (2H, m), 7.56–7.52 (2H, m), 7.01–6.88 (2H, m), 3.77–3.61 (4H, m), 2.73–2.56 (4H, m); **^{13}C NMR (150 MHz, DMSO-d_6)** δ 175.51, 151.56, 144.26, 139.10, 131.26, 131.24, 129.69, 128.02, 123.64, 117.71, 115.21, 50.50, 25.49; **ESI- HRMS** calcd. For $C_{18}H_{19}BrN_4S_2$: 435.0312. Found: 435.0304 $[M+H]^+$.

4.2.6. (E)-N-(4-bromo-2-fluorophenyl)-2-(4-thiomorpholinobenzylidene) hydrazine-1-carbo thioamide (3f)

Color: off-white; **Yield:** 86 %; **M.P.:** 198–200 °C; **FT-IR (KBr, cm^{-1}):** 3297 (N—H), 2974, 2843 (C-H), 1549 (C=N), 1278 (C=S), 1065 (C—N); **^{1}H NMR (600 MHz, DMSO-d_6)** δ 11.87 (1H, s), 9.84 (1H, s), 8.05 (1H, s), 7.74–7.67 (2H, m), 7.64 (1H, dd, *J* 9.6, 2.2), 7.54 (1H, t, *J* 8.4), 7.49–7.39 (1H, m), 7.00–6.91 (2H, m), 3.73–3.65 (4H, m), 2.69–2.61 (4H, m); **^{13}C NMR (150 MHz, DMSO-d_6)** δ 176.74, 158.45, 156.78, 151.58, 144.33, 131.97, 129.59, 127.59, 127.56, 127.51, 123.60, 119.57, 119.41, 119.32, 119.26, 115.22, 50.48, 25.49; **ESI-HRMS** calcd. For $C_{18}H_{18}BrFN_4S_2$: 453.0218. Found: 453.0211 $[M+H]^+$.

4.2.7. (E)-2-(4-thiomorpholinobenzylidene)-N-(p-tolyl)hydrazine-1-carbothioamide (3g)

Color: yellow; **Yield:** 84 %; **M.P.:** 202–204 °C; **FT-IR (KBr, cm^{-1}):** 3126 (N—H), 2974, 2906 (C-H), 1540 (C=N), 1200 (C=S), 1059 (C—N); **^{1}H NMR (600 MHz, DMSO-d_6)** δ 11.59 (1H, s), 9.90 (1H, s), 8.04 (1H, s), 7.78–7.67 (2H, m), 7.49–7.39 (2H, m), 7.16 (2H, d, *J* 8.1), 7.00–6.87 (2H, m), 3.73–3.62 (4H, m), 2.68–2.60 (4H, m), 2.31 (3H, s); **^{13}C NMR (150 MHz, DMSO-d_6)** δ 175.74, 151.49, 143.74, 137.09, 134.70, 129.58, 128.94, 126.09, 123.84, 115.26, 50.53, 25.50, 21.07; **ESI-HRMS** calcd. For $C_{19}H_{22}N_4S_2$: 371.1364. Found: 371.1354 $[M+H]^+$.

4.2.8. (E)-N-phenyl-2-(4-thiomorpholinobenzylidene)hydrazine-1-carbothioamide (3h)

Color: light brown solid; **Yield:** 82 %; **M.P.:** 225–227 °C; **FT-IR (KBr, cm^{-1}):** 3303 (N—H), 2952, 2910 (C-H), 1534 (C=N), 1199 (C=S), 1028 (C—N); **^{1}H NMR (600 MHz, DMSO-d_6)** δ 11.55 (1H, s), 9.72 (1H, s), 8.03 (1H, s), 7.73 (2H, d, *J* 8.6), 7.11 (3H, q, *J* 5.2), 6.92 (2H, d, *J* 8.7), 3.78–3.57 (4H, m), 2.76–2.54 (4H, m), 2.20 (6H, s); **^{13}C NMR (150 MHz, DMSO-d_6)** δ 176.67, 151.39, 143.13, 137.83, 136.98, 129.46, 127.99, 127.23, 124.21, 115.34, 50.61, 25.50, 18.59; **ESI-HRMS** calcd. For $C_{20}H_{24}N_4S_2$: 385.1520. Found: 385.1510 $[M+H]^+$.

4.2.9. (E)-N-Phenyl-2-(4-thiomorpholinobenzylidene)hydrazine-1-carbothioamide (3i)

Color: yellow; **Yield:** 91 %; **M.P.:** 176–178 °C; **FT-IR (KBr, cm^{-1}):** 3127 (N—H), 2960, 2831 (C-H), 1592 (C=N), 1276 (C=S), 1069 (C—N), **^{1}H NMR (600 MHz, DMSO-d_6)** δ 11.66 (1H, s), 9.92 (1H, s), 8.06 (1H, s), 7.78–7.67 (2H, m), 7.32 (1H, t, *J* 2.2), 7.26 (1H, t, *J* 8.0), 7.21 (1H, dt, *J* 8.2, 1.3), 6.98–6.90 (2H, m), 6.77 (1H, ddd, *J* 8.2, 2.6, 1.1), 3.77 (3H, s), 3.73–3.64 (4H, m), 2.68–2.58 (4H, m); **^{13}C NMR (150 MHz, DMSO-d_6)** δ 175.33, 159.44, 151.51, 143.98, 140.75, 129.65, 129.15, 123.70, 117.94, 115.23, 111.41, 110.99, 55.61, 50.51, 25.48; **ESI-HRMS** calcd. For $C_{19}H_{22}N_4OS_2$: 387.1313. Found: 387.1303 $[M+H]^+$.

4.2.10. (E)-N-(4-Methoxyphenyl)-2-(4-thiomorpholinobenzylidene) hydrazine-1-carbothioamide (3j)

Color: light yellow; **Yield:** 82 %; **M.P.:** 205–207 °C; **FT-IR (KBr, cm^{-1}):** 3319 (N—H), 2903, 2829 (C-H), 1593 (C=N), 1266 (C=S), 1076 (C—N); **^{1}H NMR (600 MHz, DMSO-d_6)** δ 11.56 (1H, s), 9.87 (1H, s), 8.04 (1H, s), 7.75–7.67 (2H, m), 7.48–7.35 (2H, m), 6.99–6.86 (4H, m), 3.77 (3H, s), 3.72–3.64 (4H, m), 2.68–2.61 (4H, m); **^{13}C NMR (150 MHz, DMSO-d_6)** δ 176.09, 157.28, 151.47, 143.61, 132.56, 129.55, 127.90, 123.90, 115.27, 113.67, 113.65, 55.70, 50.54, 25.51; **ESI-HRMS** calcd. For $C_{19}H_{22}N_4OS_2$: 387.1313. Found: 387.13034 $[M+H]^+$.

4.2.11. (E)-N-(3-Nitrophenyl)-2-(4-thiomorpholinobenzylidene) hydrazine-1-carbothioamide (3k)

Color: bright orange; **Yield:** 87 %; **M.P.:** 193–195 °C; **FT-IR (KBr, cm^{-1}):** 3155 (N—H), 2815 (C-H), 1593 (C=N), 1260 (C=S), 1025 (C—N), **^{1}H NMR (600 MHz, DMSO-d_6)** δ 11.92 (1H, s), 10.30 (1H, s), 8.67 (1H, t, *J* 2.2), 8.13 (1H, ddd, *J* 8.1, 2.0, 1.0), 8.09 (1H, s), 8.07–8.01 (1H, m), 7.80–7.71 (2H, m), 7.65 (1H, t, *J* 8.1), 7.01–6.90 (2H, m), 3.75–3.65 (4H, m), 2.69–2.60 (4H, m); **^{13}C NMR (150 MHz, DMSO-d_6)** δ 175.42, 151.63, 147.71, 144.87, 140.92, 132.04, 129.82, 129.61, 123.45, 119.93, 119.85, 115.16, 50.46, 25.47. **ESI-HRMS** calcd. For $C_{18}H_{19}N_5O_2S_2$: 402.1058. Found: 402.1051 $[M+H]^+$.

4.2.12. (E)-N-Benzyl-2-(4-thiomorpholinobenzylidene)hydrazine-1-carbothioamide (3l)

Color: brown; **Yield:** 91 %; **M.P.:** 173–175 °C; **FT-IR (KBr, cm^{-1}):** 3322 (N—H), 2999, 2910 (C-H), 1592 (C=N), 1270 (C=S), 1067 (C—N), **^{1}H NMR (600 MHz, DMSO-d_6)** δ 11.41 (1H, s), 8.93 (1H, t, *J* 6.3), 7.99 (1H, s), 7.69–7.57 (2H, m), 7.41–7.28 (4H, m), 7.28–7.18 (1H, m), 6.99–6.85 (2H, m), 4.84 (2H, d, *J* 6.3), 3.71–3.62 (4H, m), 2.69–2.56 (4H, m); **^{13}C NMR (150 MHz, DMSO-d_6)** δ 177.48, 151.40, 143.22, 140.12, 129.24, 128.61, 128.60, 127.70, 127.15, 124.06, 115.34, 50.57, 46.96, 25.50; **ESI-HRMS** calcd. For $C_{19}H_{22}N_4S_2$: 371.1364. Found: 371.1355 $[M+H]^+$.

4.2.13. (E)-N-(4-Chlorobenzyl)-2-(4-thiomorpholinobenzylidene) hydrazine-1-carbothioamide (3m)

Color: yellow; **Yield:** 93 %; **M.P.:** 170–172 °C; **FT-IR (KBr, cm^{-1}):** 3323 (N—H), 2999, 2907 (C-H), 1593 (C=N), 1270 (C=S), 1086 (C—N); **^{1}H NMR (600 MHz, DMSO-d_6)** δ 11.43 (1H, s), 8.96 (1H, t, *J* 6.3), 7.98 (1H, s), 7.69–7.59 (2H, m), 7.44–7.32 (4H, m), 6.99–6.85 (2H, m), 4.81 (2H, d, *J* 6.3), 3.72–3.62 (4H, m), 2.70–2.58 (4H, m); **^{13}C NMR (150 MHz, DMSO-d_6)** δ 177.50, 151.43, 143.34, 139.21, 131.65, 129.59, 129.26, 128.55, 124.01, 115.33, 50.56, 46.30, 25.51; **ESI-HRMS** calcd. For $C_{19}H_{21}ClN_4S_2$: 405.0974. Found: 405.0967 $[M+H]^+$.

4.2.14. (E)-N-(4-Methylbenzyl)-2-(4-thiomorpholinobenzylidene) hydrazine-1-carbothioamide (3n)

Color: yellow; **Yield:** 92 %; **M.P.:** 161–163 °C; **FT-IR (KBr, cm^{-1}):** 3315 (N—H), 2998, 2906 (C-H), 1594 (C=N), 1271 (C=S), 1091 (C—N); **^{1}H NMR (600 MHz, DMSO-d_6)** δ 11.38 (1H, s), 8.86 (1H, t, *J* 6.3), 7.98 (1H, s), 7.72–7.56 (2H, m), 7.25 (2H, d, *J* 7.8), 7.13 (2H, d, *J* 7.8), 6.99–6.83 (2H, m), 4.79 (2H, d, *J* 6.2), 3.73–3.60 (4H, m), 2.74–2.60 (4H, m), 2.28 (3H, s); **^{13}C NMR (150 MHz, DMSO-d_6)** δ 177.36, 151.39, 143.15, 137.03, 136.17, 129.22, 129.15, 127.74, 124.08, 115.35, 50.58, 46.74, 25.51, 21.18; **ESI-HRMS** calcd. For $C_{20}H_{24}N_4S_2$: 385.1520. Found: 385.1511 $[M+H]^+$.

4.2.15. (E)-N-Phenethyl-2-(4-thiomorpholinobenzylidene)hydrazine-1-carbothioamide (3o)

Color: off-white; **Yield:** 88 %; **M.P.:** 205–207 °C; **FT-IR (KBr, cm^{-1}):** 3309 (N—H), 2999, 2926 (C-H), 1597 (C=N), 1271 (C=S), 1058 (C—N); **^{1}H NMR (600 MHz, DMSO-d_6)** δ 11.33 (1H, s), 8.38 (1H, t, *J* 5.8), 7.95 (1H, s), 7.65–7.51 (2H, m), 7.34 (2H, t, *J* 7.5), 7.31–7.27 (2H, m), 7.26–7.21 (1H, m), 7.01–6.89 (2H, m), 3.76 (2H, ddd, *J* 9.5, 7.7, 5.9), 3.71–3.63 (4H, m), 2.96–2.87 (2H, m), 2.70–2.60 (4H, m); **^{13}C**

NMR (150 MHz, DMSO-d_6) δ 176.86, 151.42, 142.94, 139.78, 129.11, 129.08, 128.95, 126.68, 124.03, 115.37, 50.57, 45.40, 35.44, 25.53; **ESI-HRMS** calcd. For $C_{20}H_{24}N_4S_2$: 385.1520. Found: 385.1512 $[M + H]^+$.

4.2.16. (E)-N-Cyclohexyl-2-(4-thiomorpholinobenzylidene)hydrazine-1-carbothioamide (3p)

Color: off-white; **Yield:** 83 %; **M.P.:** 204–206 °C; **FT-IR (KBr, cm^{-1}):** 3306 (N—H), 2986, 2813 (C-H), 1507 (C=N), 1253 (C=S), 1068 (C—N), **^{1}H NMR (600 MHz, DMSO-d_6) δ** 11.22 (1H, s), 7.95 (1H, s), 7.86 (1H, d, *J* 8.6), 7.66–7.55 (2H, m), 6.98–6.87 (2H, m), 4.25–4.12 (1H, m), 3.72–3.61 (4H, m), 2.71–2.60 (4H, m), 1.92–1.82 (2H, m), 1.72 (2H, dt, *J* 13.3, 3.6), 1.61 (1H, dt, *J* 12.9, 3.6), 1.43 (2H, qd, *J* 12.3, 3.5), 1.29 (2H, qt, *J* 12.7, 3.4), 1.15 (1H, ddt, *J* 16.0, 12.4, 6.2); **^{13}C NMR (150 MHz, DMSO-d_6)** 175.64, 151.38, 143.11, 129.22, 123.95, 115.37, 52.87, 50.57, 32.39, 25.63, 25.47, 25.38. **ESI-HRMS** calcd. For $C_{18}H_{26}N_4S_2$: 363.1677. Found: 363.1669 $[M + H]^+$.

4.3. Cell culture, cell viability, and homogenization assay

The human neuroblastoma cell line SH-SY5Y (ATCC CRL-2266) and human embryonic kidney cell line HEK 293 (ATCC CRL-1573) were cultured in DMEM/F-12 medium supplemented with 10 % heat-inactivated FBS and 1 % antibiotics at 37 °C in a humidified 5 % CO_2 atmosphere. For cell viability analysis, cells (5×10 [3]/well) were seeded in 96-well plates, allowed to adhere overnight, and treated with varying compound concentrations for 24 h. Viability was assessed by crystal violet staining, elution of bound dye with sodium citrate/ethanol solution, and absorbance measurement at 600 nm, with results expressed relative to untreated controls [31]. For homogenization, cells (1×10 [6]/mL) were plated in 75 cm^2 flasks, harvested after 24 h, and lysed in buffer (0.1 M phosphate, 2 mM EDTA, 0.2 % Triton X-100, 0.3 mM ε-ACA, 1 mM DTT, 0.5 mM PMSF). Homogenization was achieved by sonication on ice, and total protein content was quantified using the BCA assay with BSA as a standard [70].

4.3.1. Cholinesterase assay

We performed cholinesterase analysis according to previously published article [71–73].

4.4. Molecular docking and dynamics studies

Molecular docking and dynamics simulations were performed using Schrödinger Molecular Modeling Software (2025–1) with the Maestro interface (v14.3) and Desmond. Protein and ligand preparations followed established group protocols [74,75]. The 3D structures of AChE (PDB ID: 4EY7) and BChE (PDB ID: 6ESJ) were obtained from the Protein Data Bank and optimized using Schrödinger's Protein Preparation Wizard, assigning bond orders, adding hydrogens, and minimizing the structures with the OPLS4 force field. Docking employed Glide XP and Induced Fit Docking (IFD), with receptor grids centered on the active site residues (grid box size: $20 \times 20 \times 20$ Å) to accommodate ligand flexibility. For each ligand, 20 docking poses were generated, and top poses were selected based on IFD scores. Prime MM-GBSA calculations with the VSGB solvation model were used to estimate binding free energies, including contributions from van der Waals, electrostatic, lipophilic, covalent, hydrogen bonding, and solvation energies. This comprehensive setup ensured accurate evaluation of ligand–protein interactions and binding affinities [76].

MD simulations used Desmond (Release 2024–3) with protein-ligand complexes in an orthorhombic box solvated by TIP4P water and neutralized with counter ions and 0.15 M NaCl. The OPLS4 force field was applied. After energy minimization and equilibration (NVT and NPT), a 100 ns production run was conducted at 300 K and 1.01325 bar using Nosé-Hoover thermostat and Martyna-Tobias-Klein barostat. Stability and conformational changes were monitored via RMSD and RMSF [75,77].

4.5. Statistical analysis

Data are presented as mean or fold change ± SD. Statistical comparisons were made using one-way ANOVA with Tukey's post hoc test (multiple groups). Analyses were performed in GraphPad Prism 9.0. Statistical significance was defined as $p < 0.05$ ($p < 0.05$: *, < 0.01: **, < 0.001: ***, < 0.0001: ****).

4.6. Limitations of the study

While this study offers important insights through synthesis, biological evaluation, and computational analysis, in vivo studies could not be conducted as it was designed as a fundamental investigation.

CRediT authorship contribution statement

Hina Aftab: Investigation, Formal analysis. **Furkan Çakır:** Investigation, Formal analysis. **Gurbet Çelik Turgut:** Investigation, Formal analysis, Data curation. **Nastaran Sadeghian:** Investigation, Formal analysis. **Rima D. Alharthy:** Investigation, Formal analysis, Data curation. **Parham Taslimi:** Investigation, Formal analysis, Data curation. **Alaattin Şen:** Resources, Investigation, Formal analysis, Data curation. **Magdi E.A. Zaki:** Investigation, Formal analysis. **Sobhi M. Gomha:** Visualization, Software, Methodology, Investigation, Formal analysis, Data curation, Conceptualization. **Javid Hussain:** Investigation, Formal analysis. **Zahid Shafiq:** Writing – review & editing, Writing – original draft, Visualization, Validation, Supervision, Resources, Methodology, Investigation, Formal analysis, Data curation, Conceptualization. **Halil Şenol:** Writing – review & editing, Writing – original draft, Visualization, Validation, Supervision, Software, Resources, Methodology, Investigation, Formal analysis, Data curation, Conceptualization.

Declaration of competing interest

The authors declare that they have no known competing financial interests or personal relationships that could have appeared to influence the work reported in this paper.

Acknowledgement

Z.S. is thankful to the ORIC, BZ University, Multan, Pakistan.

Appendix A. Supplementary data

Supplementary data to this article can be found online at https://doi.org/10.1016/j.bioorg.2025.109364.

Data availability

No data was used for the research described in the article.

References

[1] R. Hussain, H. Ullah, S. Khan, Y. Khan, T. Iqbal, R. Iqbal, H.S. Almoallim, M. J. Ansari, A promising acetylcholinesterase and butyrylcholinesterase inhibitors: in vitro enzymatic and in silico molecular docking studies of benzothiazole-based oxadiazole containing imidazopyridine hybrid derivatives, Results Chem. 7 (2024) 101503, https://doi.org/10.1016/j.rechem.2024.101503.

[2] L. Tang, L. Liu, G. Li, P. Jiang, Y. Wang, J. Li, Expression profiles of long noncoding RNAs in intranasal LPS-mediated Alzheimer's disease model in mice, Biomed. Res. Int. 2019 (1) (2019) 9642589, https://doi.org/10.1155/2019/9642589.

[3] Y. Chen, P. Yin, Q. Chen, Y. Zhang, Y. Tang, W. Jin, L. Yu, Neurodegenerative diseases and immune system: from pathogenic mechanism to therapy, Neural Regen. Res. (2025), https://doi.org/10.4103/nrr.Nrr-d-25-00274.

[4] P. Scheltens, K. Blennow, M.M.B. Breteler, B. de Strooper, G.B. Frisoni, S. Salloway, W.M. Van der Flier, Alzheimer's disease, Lancet 388 (10043) (2016) 505–517, https://doi.org/10.1016/S0140-6736(15)01124-1.

[5] X. Du, X. Wang, M. Geng, Alzheimer's disease hypothesis and related therapies, Transl. Neurodegen. 7 (2018) 2, https://doi.org/10.1186/s40035-018-0107-y.
[6] R.A. Huynh, C. Mohan, Alzheimer's disease: biomarkers in the genome, blood, and cerebrospinal fluid, Front. Neurol. 8 (2017) 102, https://doi.org/10.3389/fneur.2017.00102.
[7] G.L.S. Sousa, N.F. Nadur, L.D.P. Ferreira, T.D. Honório, A. Simon, L.M. Cabral, M.L. M. Santos, B. Andrade, E.V. de Lima, J.R. Clarke, R.N. Castro, R.O.D. Moura, A. E. Kümmerle, Discovery of novel thiosemicarbazone-acridine targeting butyrylcholinesterase with antioxidant, metal complexing and neuroprotector abilities as potential treatment of Alzheimer's disease: in vitro, in vivo, and in silico studies, Eur. J. Med. Chem. 281 (2025) 117030, https://doi.org/10.1016/j.ejmech.2024.117030.
[8] L. Muñoz-Bermejo, J. Urbano-Mairena, V. Calle-Guisado, C. Mendoza-Holgado, M. D.R. Jerez-Barroso, B. Suárez-Lantarón, J.F. López-Gil, S. Barrios-Fernández, Effects of an interdisciplinary programme on psychoemotional factors in informal caregivers of people with Alzheimer's disease, Front. Psychol. 16 (2025) 1524292, https://doi.org/10.3389/fpsyg.2025.1524292.
[9] N. Lolak, S. Akocak, M. Topal, M.Ü. Koçyiğit, M. Işık, C. Türkeş, F. Topal, M. Durgun, Ş. Beydemir, Sulfonamide-bearing pyrazolone derivatives as multitarget therapeutic agents: design, synthesis, characterization, biological evaluation, in silico ADME/T profiling and molecular docking study, Pharmacol. Res. Perspect. 13 (2) (2025) e70088, https://doi.org/10.1002/prp2.70088.
[10] Z. Köksal, H. Şenol, Anticholinesterase and carbonic anhydrase inhibitory activities of natural carnosic acid derivatives: a comprehensive in vitro and in silico study, Arch. Pharm. 358 (3) (2025) e2400909, https://doi.org/10.1002/ardp.202400909.
[11] E. Kalay, I.N. Korkmaz, F.N. Kacı, O.N. Aslan, P. Güller, F.S. Tokalı, R. Kalın, Design, synthesis, and biological studies of isoniazid-based hydrazone derivatives: antibacterial, anticancer, and enzyme inhibitory properties, Arch. Biochem. Biophys. 770 (2025) 110450, https://doi.org/10.1016/j.abb.2025.110450.
[12] R. Hussain, M. Ashraf, S. Khan, F. Rahim, W. Rehman, M. Taha, A. Sardar, Y. Khan, I. Khan, S.A.A. Shah, Molecular modeling, synthesis, and in vitro acetylcholinesterase and butyrylcholinesterase inhibitory activities of novel benzimidazole-bearing thiadiazole derivatives, J. Mol. Struct. 1295 (2024) 136582, https://doi.org/10.1016/j.molstruc.2023.136582.
[13] K. Gajendra, G.K. Pratap, D.V. Poornima, M. Shantaram, G. Ranjita, Natural acetylcholinesterase inhibitors: a multi-targeted therapeutic potential in Alzheimer's disease, Eur. J. Med. Chem. Rep. 11 (2024) 100154, https://doi.org/10.1016/j.ejmcr.2024.100154.
[14] H. Şenol, G. Çelik Turgut, A. Şen, R. Sağlamtaş, S. Tuncay, İ. Gülçin, G. Topçu, Synthesis of nitrogen-containing oleanolic acid derivatives as carbonic anhydrase and acetylcholinesterase inhibitors, Med. Chem. Res. 32 (4) (2023) 694–704, https://doi.org/10.1007/s00044-023-03031-z.
[15] G. Topcu, A. Akdemir, U. Kolak, M. Ozturk, M. Boga, F. Bahadori, S.D.H. Cakmar, Anticholinesterase and antioxidant activities of natural Abietane Diterpenoids with molecular docking studies, Curr. Alzheimer Res. 17 (3) (2020) 269–284, https://doi.org/10.2174/1567205017666200424133534.
[16] F.S. Tokalı, P. Taslimi, B. Tüzün, A. Karakuş, N. Sadeghian, İ. Gülçin, Synthesis of new carboxylates and sulfonates containing thiazolidin-4-one ring and evaluation of inhibitory properties against some metabolic enzymes, J. Iran. Chem. Soc. 20 (10) (2023) 2631–2642, https://doi.org/10.1007/s13738-023-02861-3.
[17] F.S. Tokalı, P. Taslimi, M. Sadeghi, H. Şenol, Synthesis and evaluation of Quinazolin-4(3)-one derivatives as multitarget metabolic enzyme inhibitors: a biochemistry-oriented drug design, ChemistrySelect 8 (25) (2023) e202301158, https://doi.org/10.1002/slct.202301158.
[18] F.S. Tokalı, Z. Alım, Ü. Yırtıcı, Carboxylate- and sulfonate-containing quinazolin-4 (3H)-one rings: synthesis, characterization, and carbonic anhydrase I–II and acetylcholinesterase inhibition properties, ChemistrySelect 8 (8) (2023) e202204191, https://doi.org/10.1002/slct.202204191.
[19] F.S. Tokali, P. Taslimi, I.H. Demircioglu, M. Karaman, M.S. Gultekin, K. Sendil, I. Gulcin, Design, synthesis, molecular docking, and some metabolic enzyme inhibition properties of novel quinazolinone derivatives, Arch. Pharm. (Weinheim) 354 (5) (2021) e2000455, https://doi.org/10.1002/ardp.202000455.
[20] R. Hussain, F. Rahim, H. Ullah, S. Khan, M. Sarfraz, R. Iqbal, F. Suleman, M.K. Al-Sadoon, Design, synthesis, in vitro biological evaluation and in silico molecular docking study of Benzimidazole-based oxazole analogues: a promising acetylcholinesterase and Butyrylcholinesterase inhibitors, Molecules 28 (20) (2023) 7015, https://doi.org/10.3390/molecules28207015.
[21] D. Vicente-Zurdo, B. Gómez-Gómez, I. Romero-Sánchez, N. Rosales-Conrado, M. E. León-González, Y. Madrid, Cytotoxicity, uptake and accumulation of selenium nanoparticles and other selenium species in neuroblastoma cell lines related to Alzheimer's disease by using cytotoxicity assays, TEM and single cell-ICP-MS, Anal. Chim. Acta 1249 (2023) 340949, https://doi.org/10.1016/j.aca.2023.340949.
[22] D. Tzankova, H. Kuteva, E. Mateev, D. Stefanova, A. Dzhemadan, Y. Yordanov, A. Mateeva, V. Tzankova, M. Kondeva-Burdina, A. Zlatkov, M. Georgieva, Synthesis, DFT study, and in vitro evaluation of antioxidant properties and cytotoxic and Cytoprotective effects of new Hydrazones on SH-SY5Y neuroblastoma cell lines, Pharmaceuticals 16 (9) (2023) 1198, https://doi.org/10.3390/ph16091198.
[23] S. Rajpoot, R. Kumar, R. Singh, S. Chandel, Advancements in neuroblastoma treatment: FDA-approved drugs and role of phytochemicals, Mol. Biol. Rep. 52 (1) (2025) 516, https://doi.org/10.1007/s11033-025-10633-w.
[24] R. Manikandan, K. Devi, D. Rajalingam, Synthesis and evaluation of 2, 5-substituted Pyrazolone for neuroprotective potential in SH-SY5Y human neuroblastoma cells, Indian J. Pharma. Edu. Res. 59 (1) (2025) s323–s332, https://doi.org/10.5530/ijper.20256349.
[25] L. Lopez-Suarez, S.A. Awabdh, X. Coumoul, C. Chauvet, The SH-SY5Y human neuroblastoma cell line, a relevant in vitro cell model for investigating neurotoxicology in human: focus on organic pollutants, Neurotoxicology 92 (2022) 131–155, https://doi.org/10.1016/j.neuro.2022.07.008.
[26] N.C. Colon, D.H. Chung, Neuroblastoma, Adv. Pediatr. Infect. Dis. 58 (1) (2011) 297–311, https://doi.org/10.1016/j.yapd.2011.03.011.
[27] L. Han, S. Wei, R. Wang, Y. Liu, Y. Zhong, J. Fu, H. Luo, M. Bao, Apelin-13-mediated upregulation of METTL3 ameliorates Alzheimer's disease via inhibiting Neuroinflammation through m6A-dependent regulation of lncRNA BDNF-AS, Biomolecules 15 (8) (2025) 1188, https://doi.org/10.3390/biom15081188.
[28] A. Al-Dbass, S.A. Hassan, R.S. Bhat, A.I.A. Khayyat, A. El-Ansary, Autophagy anticancer properties of *Rosmarinus officinalis* L. essential oils on the SH-SY5Y neuroblastoma cell line in vitro, IJP 19 (7) (2023) 881–892, https://doi.org/10.3923/ijp.2023.881.892.
[29] Z. Batool, G.Ö.A. Toraman, F. Çakır, G. Topçu, P. Taslimi, R.D. Alharthy, A. Khan, A. Al-Harrasi, Z. Shafiq, H. Şenol, Dual targeting of neuroblastoma and cholinesterase by morpholino/pyrrolidino-sulfonyl-indole thiosemicarbazones: synthesis, characterization, enzyme inhibition, cytotoxicity, docking and dynamics studies, Bioorg. Chem. 167 (2025) 109252, https://doi.org/10.1016/j.bioorg.2025.109252.
[30] S. Kermaninia, M. Mohammadi-Khanaposhtani, H. Şenol, F.S. Khajeh Mohammadilar, N. Dastyafteh, F. Moradkhani, S. Saeedi, B. Larijani, A. Dadgar, A. Aktaş, N. Sadeghian, P. Taslimi, M. Mahdavi, New 1E,1′E-hydrazine-bis (phenoxy-1,2,3-triazol-acetamide) derivatives as potent inhibitors against acetylcholinesterase, butyrylcholinesterase, and α-glucosidase, RSC Adv. 15 (36) (2025) 29960–29971, https://doi.org/10.1039/D5RA03877D.
[31] G.Ç. Turgut, F. Çakır, A. Şen, F.S. Tokalı, H. Şenol, Novel thiazolidinedione hybrids as cholinesterase inhibitors and targeting neuroblastoma: design, synthesis, in vitro and in silico biological evaluations, Bioorg. Chem. 164 (2025) 108869, https://doi.org/10.1016/j.bioorg.2025.108869.
[32] S. Roytrakul, J. Jaresitthikunchai, N. Phaonakrop, S. Charoenlappanit, S. Thaisakun, N. Kumsri, T. Arpornsuwan, Secretomic changes of amyloid beta peptides on Alzheimer's disease related proteins in differentiated human SH-SY5Y neuroblastoma cells, Peerj 12 (2024) e17732, https://doi.org/10.7717/peerj.17732.
[33] M.E. Arslan, H. Turkez, A. Mardinoglu, In vitro neuroprotective effects of farnesene sesquiterpene on alzheimer's disease model of differentiated neuroblastoma cell line, Int. J. Neurosci. 131 (8) (2021) 745–754, https://doi.org/10.1080/00207454.2020.1754211.
[34] H. Aftab, S. Ullah, A. Khan, M. Al-Rashida, T. Islam, K.A. Dahlous, S. Mohammad, H. Kashtoh, A. Al-Harrasi, Z. Shafiq, Design, synthesis, in vitro and in silico studies of novel piperidine derived thiosemicarbazones as inhibitors of dihydrofolate reductase, Sci. Rep. 14 (1) (2024) 22645.
[35] J. Eshal, H.Z. Tariq, J. Li, H. Aftab, H. Şenol, P. Taslimi, N. Sadeghian, R. D. Alharthy, M.S. Akram, R. Talib, Synthesis, biological evaluation, and in silico studies of phenyl naphthalene-2-sulfonate derived thiosemicarbazones as potential carbonic anhydrase inhibitors, Bioorg. Chem. 155 (2025) 108118.
[36] I. Munir, H. Aftab, A.A. Farooq, H. Şenol, P. Taslimi, N. Sadeghian, R.D. Alharthy, A. Rasool, U. Ghaffar, S. Schenone, Synthesis of 6-ethoxyphenyl 4-fluorobenzenesulfonate-tagged thiosemicarbazones as carbonic anhydrase inhibitors: in-vitro and in silico approach, Bioorg. Med. Chem. 129 (2025) 118301.
[37] Z. Batool, S.M. Dutt, M. al-Rashida, N.E. Gelsleichter, J. Pelletier, J. Sévigny, T. Islam, H. Aftab, T.M. Almutairi, F. Çakır, N-hexylsulfonyl indole based thiosemicarbazones as potent and selective ecto-5′-nucleotidase and NTPDase inhibitors, Bioorg. Chem. 163 (2025) 108717.
[38] R. Farooqi, S. Ullah, A. Khan, S.S. Gurav, S.N. Mali, H. Aftab, M.K. Al-Sadoon, M.-H. Hsu, P. Taslimi, A. Al-Harrasi, Design, synthesis, in-vitro and in-silico studies of novel N-heterocycle based hydrazones as α-glucosidase inhibitors, Bioorg. Chem. 156 (2025) 108155.
[39] H. Aftab, S. Ullah, A. Khan, M. Al-Rashida, T. Islam, A. Alshammari, N.A. Albekairi, P. Taslimi, A. Al-Harrasi, Z. Shafiq, Synthesis, in vitro biological evaluation and in silico studies of novel pyrrolidine derived thiosemicarbazones as dihydrofolate reductase inhibitors, RSC Adv. 14 (43) (2024) 31409–31421.
[40] R. Hussain, S. Khan, A. Sardar, L. Rasheed, M.S. Islam, T.M. Almutairi, Synthetic strategies, biological and computational screening of thiadiazole bearing benzothiazole derivatives as prospective anti-diabetic agents, J. Mol. Struct. 1337 (2025) 142141, https://doi.org/10.1016/j.molstruc.2025.142141.
[41] R. Hussain, W. Rehman, S. Khan, F. Jaber, F. Rahim, M. Shah, Y. Khan, S. Iqbal, H. Naz, I. Khan, M. Issa Alahmdi, N.S. Awwad, H.A. Ibrahium, Investigation of novel bis-thiadiazole bearing schiff base derivatives as effective inhibitors of thymidine phosphorylase: Synthesis, in vitro bioactivity and molecular docking study, Saudi Pharm. J. 31 (11) (2023) 101823, https://doi.org/10.1016/j.jsps.2023.101823.
[42] A. Farzaliyeva, H. Şenol, P. Taslimi, F. Çakır, V. Farzaliyev, N. Sadeghian, I. Mamedov, A. Sujayev, A. Maharramov, S. Alwasel, İ. Gulçin, Synthesis and biological studies of acetophenone-based novel chalcone, semicarbazone, thiosemicarbazone and indolone derivatives: structure-activity relationship, molecular docking, molecular dynamics, and kinetic studies, J. Mol. Struct. 1321 (2025) 140197, https://doi.org/10.1016/j.molstruc.2024.140197.
[43] A.B.M. Ibrahim, P. Mayer, S.M. Abbas, Thiosemicarbazones and derived tin complexes: synthesis, structural analysis and in vitro evaluation against bacterial and cancer cells, Appl. Organomet. Chem. 38 (9) (2024), https://doi.org/10.1002/aoc.7620.
[44] A. Nicolás, J.G. Quero, M. Barroso, Z. Gandara, L. Gude, DNA interactions and biological activity of 2,9-Disubstituted 1,10-Phenanthroline Thiosemicarbazone-

based ligands and a 4-Phenylthiazole derivative, Biology-Basel 13 (1) (2024) 60, https://doi.org/10.3390/biology13010060.
[45] F.S. Tokalı, H. Şenol, T.G. Katmerlikaya, A. Dağ, K. Şendil, Novel thiosemicarbazone and thiazolidin-4-one derivatives containing vanillin core: synthesis, characterization, and anticancer activity studies, J. Heterocyclic Chem. 60 (4) (2023) 645–656, https://doi.org/10.1002/jhet.4619.
[46] T. Alagoz, F.G. Caliskan, H.G. Bilgicli, M. Zengin, M. Sadeghi, P. Taslimi, I. Gulcin, Synthesis, characterization, biochemical, and molecular modeling studies of carvacrol-based new thiosemicarbazide and 1,3,4-thiadiazole derivatives, Arch. Pharm. (Weinheim) 356 (12) (2023) e2300370, https://doi.org/10.1002/ardp.202300370.
[47] F. Rahim, H. Ullah, M. Taha, R. Hussain, M. Sarfraz, R. Iqbal, N. Iqbal, S. Khan, S.A. A. Shah, M.A. Albalawi, M.A. Abdelaziz, F.S. Alatawi, A. Alasmari, M.I. Sakran, N. Zidan, I. Jafri, K.M. Khan, Synthesis of new Triazole-based Thiosemicarbazone derivatives as anti-Alzheimer's disease candidates: evidence-based in vitro study, Molecules 28 (1) (2023) 21, https://doi.org/10.3390/molecules28010021.
[48] D.D.S. Oliveira, T. Lapierre, F.C. Silva, I.V. Cunha, R.A.C. Souza, P.A. Matos, G. M. Almeida, C.G. Oliveira, T.G. Araújo, T.M. Tsubone, C.O. Rezende Jr., Advances in breast Cancer drug discovery: a review of therapeutic strategies and studies involving photosensitizers, caged Xanthones and Thiosemicarbazones derivatives, J. Braz. Chem. Soc. (2023), https://doi.org/10.21577/0103-5053.20230128.
[49] F.S. Tokalı, P. Taslimi, H. Usanmaz, M. Karaman, K. Sendil, Synthesis, characterization, biological activity and molecular docking studies of novel schiff bases derived from thiosemicarbazide: biochemical and computational approach, J. Mol. Struct. 1231 (2021) 129666, https://doi.org/10.1016/j.molstruc.2020.129666.
[50] R. Hussain, W. Rehman, F. Rahim, A.M. Mahmoud, M.M. Alanazi, S. Khan, L. Rasheed, I. Khan, Synthetic transformation of 6-Fluoroimidazo[1,2-a]Pyridine-3-carbaldehyde into 6-Fluoroimidazo[1,2-a]pyridine-oxazole derivatives: in vitro urease inhibition and in silico study, Saudi Pharm. J. 31 (8) (2023) 101667, https://doi.org/10.1016/j.jsps.2023.05.026.
[51] S. Kumar, P. Bishnoi, N. Chauhan, P. Kumar, R. Aggarwal, Therapeutic potential of morpholine-based compounds in neurodegenerative diseases: SAR insights and analysis, Future Med. Chem. (2025), https://doi.org/10.1080/17568919.2025.2515812.
[52] A. Behcet, P. Taslimi, B. Sen, T. Taskin-Tok, A. Aktas, Y. Gok, M. Aygun, I. Gulcin, New palladium complexes with N-heterocyclic carbene and morpholine ligands: synthesis, characterization, crystal structure, molecular docking, and biological activities, J. Biochem. Mol. Toxicol. 38 (1) (2024) e23554, https://doi.org/10.1002/jbt.23554.
[53] F.S. Tokalı, H. Şenol, Ş. Ateoglu, F. Akbaş, A series of quinazolin-4(3H)-one-morpholine hybrids as anti-lung-cancer agents: synthesis, molecular docking, molecular dynamics, ADME prediction and biological activity studies, Chem. Biol. Drug Des. 104 (1) (2024) e14599, https://doi.org/10.1111/cbdd.14599.
[54] D. Zolotareva, A. Zazybin, A. Dauletbakov, Y. Belyankova, B.G. Parache, S. Tursynbek, T. Seilkhanov, A. Kairullinova, Morpholine, Piperazine, and Piperidine derivatives as antidiabetic agents, Molecules 29 (13) (2024) 3043, https://doi.org/10.3390/molecules29133043.
[55] A. Kumari, R.K. Singh, Morpholine as ubiquitous pharmacophore in medicinal chemistry: deep insight into the structure-activity relationship (SAR), Bioorg. Chem. 96 (2020) 103578, https://doi.org/10.1016/j.bioorg.2020.103578.
[56] R. Hussain, W. Hassan, F. Rahim, S. Subhan, Z. Subhan, S. Khan, A. Hussain, H. Ullah, M. Nabi, R. Ullah, E.A. Ali, S. Aghayeva, Pyrazine based novel molecules as potential therapeutic agents: synthesis, in vitro biological screening, in silico ADMET profiling and molecular docking study, Results Chem. 10 (2024) 101698, https://doi.org/10.1016/j.rechem.2024.101698.
[57] B. Kurban, D. Osmaniye, B.N. Sağlık Özkan, Z.A. Kaplancıklı, Investigation of dual AChE/MAO inhibitory activities of new morpholine and piperazine structured compounds, Eur. J. Life Sci. 3 (2) (2024) 55–65, https://doi.org/10.55971/EJLS.1497639.
[58] Y.H. Chen, X.Y. Hou, D.F. Zhi, C. Li, T. Tian, J.Y. Sun, L.X. Zhao, C.H. Zhao, Synthesis, characterization and anticancer activity of Oleanolic acid and Ursolic acid derivatives, Chin. J. Org. Chem. 36 (4) (2016) 795–802, https://doi.org/10.6023/cjoc201509002.
[59] V. Kr, Shameemunnisa, S. SyedShafi, Synthesis, Characterization and Antimicrobial Evaluation of Novel 2-Pyrazoline Derivatives Containing Morpholine Moiety, 2017.
[60] T. El Malah, A.A. El-Rashedy, O. Kutkat, R.A. El Shesheny, A.E. Rashad, A. H. Shamroukh, Synthesis of isatin-schiff base and 1, 2, 3-Triazole hybrids as anti-SARS-CoV-2 agents: DFT, molecular docking, and ADMET studies, Polycycl. Aromat. Compd. (2025) 1–26.
[61] N. Sharon, V.G. Ugale, P. Padmaja, D. Lokwani, C. Salunkhe, P. Shete, P.N. Reddy, P.P. Kulkarni, Development of novel 9 H-carbazole-4 H-chromene hybrids as dual cholinesterase inhibitors for the treatment of Alzheimer's disease, Mol. Divers. 29 (1) (2025) 379–396.
[62] M.B. Tehrani, Z. Rezaei, M. Asadi, H. Behnammanesh, H. Nadri, F. Afsharirad, A. Moradi, B. Larijani, M. Mohammadi-Khanaposhtani, M. Mahdavi, Design, synthesis, and cholinesterase inhibition assay of coumarin-3-carboxamide-N-morpholine hybrids as new anti-alzheimer agents, Chem. Biodivers. 16 (7) (2019) e1900144.
[63] Y.S. Kumar, M. Malviya, J.N.S. Chandra, C. Sadashiva, C.A. Kumar, S.B. Prasad, D. Prasanna, M. Subhash, K. Rangappa, Effect of novel N-aryl sulfonamide substituted 3-morpholino arecoline derivatives as muscarinic receptor 1 agonists in Alzheimer's dementia models, Bioorg. Med. Chem. 16 (9) (2008) 5157–5163.
[64] R. Sasidharan, B.H. Eom, J.H. Heo, J.E. Park, M.A. Abdelgawad, A. Musa, N. Gambacorta, O. Nicolotti, S.L. Manju, B. Mathew, Morpholine-based chalcones as dual-acting monoamine oxidase-B and acetylcholinesterase inhibitors: synthesis and biochemical investigations, J. Enzyme Inhib. Med. Chem. 36 (1) (2021) 188–197.
[65] S. Hashmi, S. Khan, Z. Shafiq, P. Taslimi, M. Ishaq, N. Sadeghian, H.S. Karaman, N. Akhtar, M. Islam, A. Asari, Probing 4-(diethylamino)-salicylaldehyde-based thiosemicarbazones as multi-target directed ligands against cholinesterases, carbonic anhydrases and α-glycosidase enzymes, Bioorg. Chem. 107 (2021) 104554.
[66] M. Erdoğan, M. Serdar Çavuş, H. Muğlu, H. Yakan, C. Türkeş, Y. Demir, Ş. Beydemir, Synthesis, theoretical, in silico and in vitro biological evaluation studies of new thiosemicarbazones as enzyme inhibitors, Chem. Biodivers. 20 (11) (2023) e202301063.
[67] G.E. Mathew, J.M. Oh, K. Mohan, A. Tengli, B. Mathew, H. Kim, Development of methylthiosemicarbazones as new reversible monoamine oxidase-B inhibitors for the treatment of Parkinson's disease, J. Biomol. Struct. Dyn. 39 (13) (2021) 4786–4794.
[68] S. Jalil, R. Basri, M. Aziz, Z. Shafiq, S.A. Ejaz, A. Hameed, J. Iqbal, Pristine 2-chloroquinoline-based-thiosemicarbazones as multitarget agents against alzheimer's disease: in vitro and in silico studies of monoamine oxidase (MAO) and cholinesterase (ChE) inhibitors, J. Mol. Struct. 1306 (2024) 137841.
[69] N. Kılınç, M. Açar, S. Tuncay, Ö.F. Karasakal, Identification of potential inhibitors for severe acute respiratory syndrome-related coronavirus 2 (SARS-CoV-2) angiotensin-converting enzyme 2 and the Main protease from Anatolian traditional plants, Lett. Drug. Des. Discov. 19 (11) (2022) 996–1006, https://doi.org/10.2174/1570180819666211230123145.
[70] G.Ç. Turgut, D. Doyduk, Y. Yıldırır, S. Yavuz, A. Akdemir, A. Dişli, A. Şen, Computer design, synthesis, and bioactivity analyses of drugs like fingolimod used in the treatment of multiple sclerosis, Bioorg. Med. Chem. 25 (2) (2017) 483–495, https://doi.org/10.1016/j.bmc.2016.11.015.
[71] F.S. Tokali, P. Taslimi, B. Tuzun, A. Karakus, N. Sadeghian, I. Gulcin, Novel Quinazolinone derivatives: potential synthetic analogs for the treatment of Glaucoma, Alzheimer's disease and diabetes mellitus, Chem. Biodivers. 20 (10) (2023) e202301134, https://doi.org/10.1002/cbdv.202301134.
[72] P. Taslimi, M. Işık, F. Türkan, M. Durgun, C. Türkeş, İ. Gülçin, Ş. Beydemir, Benzenesulfonamide derivatives as potent acetylcholinesterase, α-glycosidase, and glutathione S-transferase inhibitors: biological evaluation and molecular docking studies, J. Biomol. Struct. Dyn. 39 (15) (2021) 5449–5460, https://doi.org/10.1080/07391102.2020.1790422.
[73] P. Taslimi, H. Akincioglu, I. Gulcin, Synephrine and phenylephrine act as alpha-amylase, alpha-glycosidase, acetylcholinesterase, butyrylcholinesterase, and carbonic anhydrase enzymes inhibitors, J. Biochem. Mol. Toxicol. 31 (11) (2017), https://doi.org/10.1002/jbt.21973.
[74] I. Mamedov, H. Şenol, F. Naghiyev, V. Khrustalev, N. Sadeghian, P. Taslimi, New tetrahydro-isoquinoline derivatives as cholinesterase and α-glycosidase inhibitors: synthesis, characterization, molecular docking & dynamics, ADME prediction, in vitro cytotoxicity and enzyme inhibition studies, J. Mol. Liq. 404 (2024) 125006, https://doi.org/10.1016/j.molliq.2024.125006.
[75] B. Zengin Kurt, M. Gökçe, H. Şenol, D. Öztürk Civelek, G. Dandin, I. Gazioglu, Synthesis, cytotoxic evaluation, and in silico studies of novel benzenesulfonamide-thiazolidinone derivatives against colorectal carcinoma, J. Mol. Struct. 1321 (2025) 140153, https://doi.org/10.1016/j.molstruc.2024.140153.
[76] O.G.V. Petrova, D.N. Tomilin, H. Şenol, K.V. Belyaeva, L.P. Nikitina, L.A. Oparina, L.N. Sobenina, B.A. Trofimov, N. Sadeghian, P. Taslimi, V. Farzaliyev, A. Sujayev, İ. Gulçin, Synthesis of pyrrole-heterocyclic derivatives as anti-Alzheimer and antidiabetic candidates: an in vitro-in silico study, J. Mol. Struct. 1315 (2024) 138998, https://doi.org/10.1016/j.molstruc.2024.138998.
[77] E.N. Ay, F. Çakır, S. Akyüz, N. Kılınç, F.S. Tokalı, H. Şenol, Synthesis, characterization, in vitro and in silico investigations of novel 1,2,3-triazole substituted salicylic acid phenolic hydrazones hybrids targeting TGF-β2 expression in colorectal carcinoma, Eur. J. Med. Chem. 296 (2025) 117915, https://doi.org/10.1016/j.ejmech.2025.117915.